International Journal of Heat and Mass Transfer 195 (2022) 123200

Contents lists available at ScienceDirect

International Journal of Heat and Mass Transfer

journal homepage: www.elsevier.com/locate/hmt

Subcooled flow boiling heat transfer in a partially-heated rectangular channel at different orientations in Earth gravity

V.S. Devahdhanush, Issam Mudawar*

Purdue University Boiling and Two-Phase Flow Laboratory (PU-BTPFL), School of Mechanical Engineering, Purdue University, 585 Purdue Mall, West Lafayette, IN 47907, USA

ARTICLE INFO

Article history:
Received 15 May 2022
Revised 10 June 2022
Accepted 25 June 2022
Available online 8 July 2022

Keywords:
Subcooled flow boiling
Two-phase heat transfer coefficient
Orientation effects
Partial heating
Fully developed boiling
Nucleate boiling degradation

ABSTRACT

This study explores subcooled flow boiling of n-Perfluorohexane in a rectangular channel of 5.0 mm height, 2.5 mm width (heated), and 114.6 mm heated length. This Flow Boiling Module (FBM) is part of the Flow Boiling and Condensation Experiment (FBCE), which is a long-term collaborative effort to study the effects of gravity on flow boiling and condensation for their implementation in future space missions besides other applications. Datasets obtained from subcooled-inlet experiments performed using the FBM prior to its launch to the International Space Station (ISS) are examined and local subcooled flow boiling datapoints compiled to form a consolidated database. The consolidated 2589 datapoints cover broad ranges of operating conditions (mass velocity: 172.79 – 3200.00 kg/m^{2}s, pressure: 102.16 – 238.44 kPa, subcooling: 0.13 – 34.93°C, quality: -0.560 – -0.000, heat flux: 1.80 – 49.99 W/cm^2), flow orientations (vertical upflow, vertical downflow, and horizontal flow in Earth gravity), and partial heating configurations (single- and double-sided heating). Prior seminal correlations for subcooled flow boiling heat transfer are assessed for their predictive performance. Each local flow boiling curve is analyzed and manually demarcated into three regimes: partially developed boiling (PDB), fully developed boiling (FDB), and nucleate boiling degradation (NBD). A simple, yet very effective correlation based on dimensionless groups and having a fully explicit functional form, is developed. The new correlation well predicts both the subcooled flow PDB and FDB regimes with overall mean absolute errors (MAEs) of 9.59% and 6.91%, respectively. Although predictions for the NBD regime are much higher than observed with an overall MAE of 41.71%, they can be treated as upper limits to heat transfer here. The correlation is independent of both flow orientation and heating configuration. Overall, the new correlation clearly outperforms all prior seminal correlations for the entire consolidated database, with excellent predictions for both partially and fully developed subcooled flow boiling, *i.e.*, for heat fluxes ranging from onset of nucleate boiling to onset of nucleate boiling degradation.

1. Introduction

1.1. Two-phase flows and heat transfer in space applications

Several space agencies around the world, including NASA, are planning future space missions that are expected to be for longer durations and distances. Space vehicles and equipment used in such missions would need to be suited for different gravity environments as they travel from Earth gravity to microgravity and possibly hyper-gravities. Thermal management systems used in such missions also face this constraint. It is well established that single-phase thermal management schemes are unable to cater to the high heat transfer rates demanded by these applications. This brings into effect two-phase schemes, that offer far better heat transfer rates while keeping the system at safe low temperatures, by operating through combined sensible and latent heat transfer. Over the years, the Purdue University Boiling and Two-Phase Flow Laboratory (PU-BTPFL) has investigated several two-phase schemes, including evaporating films [1], pool boiling [2], flow boiling in macro-channels [3,4], micro-channels [5,6], and annuli [7], spray cooling [8], jet impingement cooling [9,10], and hybrids between the aforementioned schemes [11]. Several predictive and design tools for these schemes have been developed. Besides the thermal control systems of space vehicles, two-phase flows can also be used in fission power systems coupled with the Rankine power cycle [12,13].

* Corresponding author.
E-mail address: mudawar@ecn.purdue.edu (I. Mudawar).
URL: https://engineering.purdue.edu/BTPFL (I. Mudawar)

https://doi.org/10.1016/j.ijheatmasstransfer.2022.123200
0017-9310/

Nomenclature

A_c	cross-sectional area
Bo	boiling number, $q"_w/(Gh_{fg})$
C, C_1, C_2, C_3	constants
c_p	specific heat at constant pressure
D	diameter
D_h	hydraulic diameter
G	mass velocity
g	gravitational acceleration
g_e	gravitational acceleration on Earth
H	larger dimension of channel's cross section
h	enthalpy; heat transfer coefficient
h_{fg}	latent heat of vaporization
Ja^{**}	modified Jacob number, $c_{p,f}\Delta T_{sub}/h_{fg}$
k	thermal conductivity
L_d	upstream development length
L_e	downstream exit length
L_h	heated length
$\dot{m}$	mass flow rate
N	number of datapoints
Nu	Nusselt number, hD_h/k_f
P_h	heated perimeter
Pr	Prandtl number
p	pressure
$q"$	heat flux
$q"_{CHF}$	critical heat flux
Re_{fo}	liquid-only Reynolds number, GD_h/μ_f
T	temperature
ΔT_{sub}	fluid subcooling, T_{sat} - T_f
W	smaller dimension of channel's cross section
x_e	thermodynamic equilibrium quality
z	streamwise coordinate

Greek symbols

θ	orientation angle of heated wall
μ	dynamic viscosity
ξ_{15}, ξ_{30}, ξ_{50}	percentage of datapoints predicted within ±15%, ±30%, ±50% errors, respectively
ρ	density

Subscripts

a	denotes wall 1 or 2 (= 1 or 2)
exp	experimental value
f	liquid; bulk fluid
fo	liquid-only
g	vapor
HSI	for highly subcooled inlet
h	heated
in	channel heated section inlet
NSI	for near-saturated inlet
ONB	corresponding to ONB
$ONBD$	corresponding to ONBD
out	channel heated section outlet
$pred$	predicted value
sat	saturation
sc	subcooled
sp	single-phase (liquid in this study)
w	wall
wa	wall 1 or 2 (= $w1$ or $w2$)
$x=0$	corresponding to the location where $x_e = 0$
z	local (along streamwise direction)

Acronyms

CHF	Critical Heat Flux
DNB	Departure from Nucleate Boiling
FBCE	Flow Boiling and Condensation Experiment
FBM	Flow Boiling Module
FDB	Fully Developed Boiling
ISS	International Space Station
MAE	Mean Absolute Error (%)
MST	Mission Sequence Testing
nPFH	n-Perfluorohexane
NBD	Nucleate Boiling Degradation
ONB	Onset of Nucleate Boiling
ONBD	Onset of Nucleate Boiling Degradation
PDB	Partially Developed Boiling
RMSE	Root Mean Square Error (%)

1.2. Gravitational effects on two-phase flows and heat transfer

Large differences in densities between the two phases necessitate the understanding of the effects of gravity on heat transfer and flow physics of two-phase thermal management schemes. Several researchers have studied this aspect by performing two-phase experiments at different flow orientations in Earth gravity [4], using drop towers [14], onboard aircrafts executing parabolic maneuvers [15], sounding/ballistic rockets [16], and onboard space stations orbiting the Earth [17]. Amongst these studies, very few have focused on flow boiling in microgravity. The cheapest method is to collect data at different channel orientations on the ground, *i.e.*, under Earth gravity.

The most common flow boiling orientations experimented in Earth gravity include vertical upflow, vertical downflow, and horizontal flow. Among these, vertical upflow benefits the most from gravitational effects due to buoyancy aiding vapor removal from the channel, increased flow acceleration, enhanced flow stability, and Critical Heat Flux (CHF) [18]. On the other hand, gravity hampers vertical downflow the most, due to buoyancy retarding the escape of produced vapor out of the channel resulting in flow deceleration, reduced CHF, and possible stagnation and choking. Horizontal flows are moderately affected by gravity and the thermal behavior lies in between vertical upflow and downflow. In horizontal flows, the produced vapor stratifies at the top of the channel, resulting in a vapor layer insulting a majority of the top wall; this results in degraded nucleate boiling heat transfer and reduced CHF at the top wall, while the bottom wall remains unobstructed for boiling. Gravitational effects are only prominent at low flow inertia where the forced fluid flow is not effectively able to push out the produced vapor from the channel; however, at high flow inertia, the thermal limit of two-phase flows, CHF, becomes identical for all orientations [19,20].

1.3. Subcooled flow boiling

Most flow boiling applications utilize fluid in subcooled liquid state in order to capitalize on the high condensing capability of the bulk fluid during subcooled flow boiling. Note that depending on the channel geometry and operating conditions, subcooled flow boiling could transition to saturated flow boiling when the local fluid temperature reaches the saturation temperature at local pressure. Subcooled flow boiling offers enhanced CHF and heat transfer rates, and much lower pressure drop than saturated flow boiling [21].

A schematic representation of a typical local flow boiling curve for subcooled inlet conditions is shown in Fig. 1, with key regions and transition points indicated. Starting from zero, as wall heat flux is incremented, wall temperature linearly increases due to single-phase liquid convection having an almost constant heat

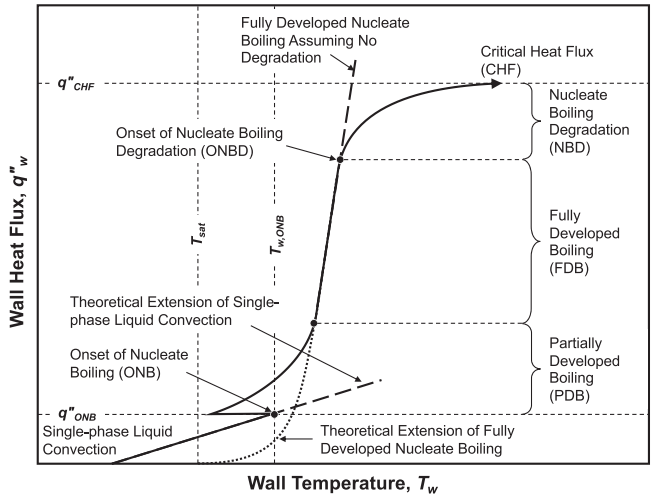

Fig. 1. Typical flow boiling curve for subcooled inlet conditions with key regimes and transition points indicated.

transfer coefficient. This linear behavior ends when bubbles start nucleating on the wall, *i.e.*, at Onset of Nucleate Boiling (ONB). Note that in most cases, the wall superheat will drop after ONB; although this was observed in the transient data during the present experiments [22], this was not captured in the steady-state averaged data due to heat flux increments being coarser near ONB. After ONB, the heat transfer coefficient and therefore the slope of the curve enormously increases and the curve becomes almost vertical and linear. Nucleate boiling has fully developed in this region and the curve superimposes onto the pure fully developed nucleate boiling curve; this region is termed Fully Developed Boiling (FDB) and the lower transitory region is termed Partially Developed Boiling (PDB). Upon further increasing heat flux, the Onset of Nucleate Boiling Degradation (ONBD) point is reached, where the boiling curve starts deviating from the fully developed nucleate boiling curve and its slope decreases until zero. Here, large portions of the wall experience intermittent and/or partial blanketing by large coalesced vapor structures/layers, resulting in reduced availability of liquid at the wall for further boiling [10]. For practical thermal management applications, the curve terminates at the CHF point (also called Departure from Nucleate Boiling, DNB, in subcooled flow boiling), when the wall temperature drastically increases for small increases in wall heat flux. At CHF, nucleate boiling completely transitions to film boiling, meaning a large continuous vapor layer exists along the heated wall and heat transfer occurs by conduction and radiation through the vapor film and phase change at the liquid-vapor interface. The regime between ONBD and CHF is designated Nucleate Boiling Degradation (NBD).

1.4. Predictive methods for subcooled flow boiling heat transfer

The first correlation for fully developed subcooled flow boiling was probably proposed by McAdams *et al.* [23] in 1949. By a simple power law fit to their boiling curves obtained for water, they proposed

$$q''_w = C(T_w - T_{sat})^{3.86}, \quad (1)$$

where C is an empirical constant, which varied with the amount of non-condensable gases dissolved. Thereafter, several investigators conducted subcooled flow boiling experiments using water and proposed modifications to the dimensional power law fit; some notable ones include Jens and Lottes [24], Thom *et al.* [25], Araki *et al.* [26], and Hata and Masuzaki [27]. The main drawback of this type of correlations is their applicability to very narrow ranges of experiments; in fact, almost all of them were developed for water alone.

Besides power law fits, several correlations exist in the literature for predicting the heat transfer coefficient for subcooled flow boiling. These can be broadly classified into three: (i) correlations based on dimensionless group analysis (*e.g.*, Papell [28], Badiuzzaman [29], Hodgson [30], Moles and Shaw [31], Shaw [32]), (ii) correlations based on superposition (interpolation/asymptotic combination) of single-phase convection and nucleate boiling heat transfer correlations (similar to Chen's [33] correlation for saturated boiling; *e.g.*, Bjorg *et al.* [34], Gungor and Winterton [35], Liu and Winterton [36]), and (iii) correlations that have characteristics of the other types and have intermediate forms (*e.g.*, Shah [37,38]). The first has been shown to yield more accurate predictions for both partially and fully developed boiling although they are not directly derived from flow physics, whereas the second is based on several averaging techniques between single-phase liquid convection and pool boiling nucleate boiling heat transfer coefficients multiplied by certain factors. The third can also be viewed as enhancement type correlations, where single-phase heat transfer coefficient is multiplied by certain empirically derived factors, in which aspect they are closer to dimensionless group correlations, although they are presented in a dimensional form similar to power law fits.

Select seminal correlations [28,29,31,32,35–38] for subcooled flow boiling heat transfer coefficient, which were developed based on consolidated databases containing at least two significantly different fluids, are assessed in this study. Besides these, several other correlations exist in the literature based on very narrow ranges of experimental data for specific applications (i) using water, such as Prodanovic *et al.* [39] and Baburajan *et al.* [40] based on dimensionless groups, Hua *et al.* [41], Yan *et al.* [42], and Zhu *et al.* [43] of the superposition type, and Chen *et al.* [44] based on Shah's [38] correlation, (ii) using refrigerants (R-11 and R-123) such as Haynes and Fletcher [45] of the superposition type, and (iii) using specialized heat transfer fluids (HFE-7100) such as Lee and Mudawar [46] based on both Shah's [37] and dimensionless groups.

1.5. Objectives of study

This study is part of a long-term collaborative effort between PU-BTPFL and the NASA Glenn Research Center to study flow boiling and condensation in microgravity. Since 2012, the ultimate goal has been to develop the Flow Boiling and Condensation Experiment (FBCE) for the International Space Station (ISS). During these years, several flow boiling experiments have been conducted and a large number of datapoints amassed for different flow orientations in Earth gravity. Even though flow boiling physics has been discussed in detail [22,47,48], CHF models [49,50] and correlations [51] developed, and transient behavior analyzed [4,52], detailed predictive analysis of flow boiling heat transfer has not been done. This study aims at (i) consolidating datapoints for subcooled flow boiling heat transfer coefficient to cover broad ranges of operating conditions, flow orientations, and partial heating configurations, (ii) assessing the predictive capability of prior correlations for this consolidated database, and (iii) proposing a new correlation, that is simple yet very effective for all flow orientations and partial heating configurations.

2. Experimental Methods

As the FBCE system was developed over the years, the flow loop was slightly modified to improve its performance and reliability. Since the present study uses data from different versions of the FBCE system, only a brief overview of the experimental methods is

Table 1
Summary of experimental cases considered in this study.

Dataset	MST (2021) data	MST (2021) data	2016 data	2016 data	2016 data	Overall
Flow orientation	Vertical up	Vertical up	Vertical up	Vertical down	Horizontal	
Heating configuration	Single-sided	Double-sided	Double-sided	Double-sided	Double-sided	
Mass flow rate, $\dot{m}$ [g/s]	2.25 – 40.00	2.25 – 40.00	2.16 – 30.49	2.52 – 30.00	2.29 – 30.65	2.16 – 40.00
Mass velocity, G [kg/m^{2}s]	179.60 – 3199.98	179.65 – 3200.00	172.69 – 2438.94	201.85 – 2399.31	182.85 – 2452.39	172.69 – 3200.00
FBM inlet pressure, p_{in} [kPa]	119.02 – 171.17	118.61 – 190.81	108.02 – 229.77	123.83 – 239.48	98.46 – 196.18	98.46 – 239.48
Inlet saturation temperature, $T_{sat,in}$ [°C]	61.96 – 73.55	61.86 – 77.21	58.82 – 83.37	62.95 – 84.84	56.08 – 77.87	56.08 – 84.84
Inlet fluid temperature, T_{in} [°C]	34.01 – 71.60	34.89 – 72.95	25.90 – 66.44	27.93 – 66.68	23.15 – 56.54	23.15 – 72.95
Inlet subcooling, $\Delta T_{sub,in}$ [°C]	0.24 – 31.77	0.18 – 32.00	15.36 – 36.44	17.10 – 37.31	16.88 – 35.42	0.18 – 37.31
Inlet quality, $x_{e,in}$	-0.421 – -0.003	-0.429 – -0.002	-0.572 – -0.166	-0.539 – -0.185	-0.532 – -0.183	-0.572 – -0.002

discussed here, noting differences in the flow loop between different datasets.

For further details on the different components, instrumentation, measurement uncertainties, operating procedure, imaging technique, *etc*., the reader is referred to the original publications where these experiments were first presented. This includes Mission Sequence Testing (MST, the final pre-launch ground experiments conducted in Earth gravity using the same system that was launched to the ISS) [22], and ground experiments conducted in 2016 (a different system but similar test module) [4]. Although parabolic-flight microgravity experiments were conducted in 2013 for subcooled inlet [15], this data is not included in the present consolidated database due to the experiments having focused on solely capturing the upper portion of the boiling curves near CHF (*i.e*., from around ONBD to CHF). A summary of all experimental cases with subcooled inlet considered in this study is presented in Table 1.

2.1. Flow boiling module

The test module used in this study, called the Flow Boiling Module (FBM), is schematically represented in Fig. 2(a). It is primarily made of three transparent polycarbonate plates sandwiched between two aluminum plates and bolted together. A rectangular flow channel of 5.0-mm × 2.5-mm ($H \times W$) cross section is milled into the middle polycarbonate plate. On either side of the channel are inserted copper strips of dimensions 114.6-mm length, 15.5-mm width, and 1.04-mm thickness. The construction of these copper strips is portrayed in Fig. 2(b), with details on how six resistive heaters each are affixed to their undersides. As shown in Fig. 2(c), the tips of the strip thermocouples are placed 0.48 mm away from the heating surface and the resistive heaters are placed 0.56 mm away from the heating surface. The flow channel within the FBM consists of 3 streamwise sections: an upstream 327.7-mm-long adiabatic development length, a middle 114.6-mm-long heated length, and a downstream 60.7-mm-long adiabatic length. A high-speed camera is used to capture images of the flow within the FBM's heated section at a frequency of 2000 frames per second.

2.2. Flow loop

A schematic of the most recent version of the flow loop, used for MST, is shown in Fig. 3. Pure n-Perfluorohexane (nPFH, C_6F_{14}) was used for MST, whereas commercial FC-72 was used for the 2016 experiments (note that the thermophysical properties of both fluids are very similar to each other, and they are selected for their potential in space applications [53]). The working fluid is positively displaced through the closed flow loop at a particular flow rate using an internal gear pump, which receives feedback from a Coriolis flow meter located immediately downstream of the pump. The fluid then passes through a filter and a preheater (Bulk Heater Module), which helps set a particular inlet subcooling. The subcooled liquid undergoes subcooled flow boiling within the FBM and, depending on the operating conditions, exits as a subcooled or saturated liquid-vapor mixture. This is condensed back to a subcooled liquid in a condenser and, to ensure thermodynamic equilibrium, passed through a static mixer. Downstream of the mixer is a T-junction where an accumulator is connected to the main flow loop and helps set the system pressure and suppress flow loop instabilities [54]. A degassing contactor is connected in parallel to the main flow loop and periodically helps remove any non-condensable gases dissolved in the working fluid.

Some aspects in which the 2016 flow loop differs from the most-recent (MST) flow loop include: (i) the 2016 loop components needed manual operation whereas the recent loop is capable of remote operation and via feedback from sensors, (ii) turbine flow meter was used in place of Coriolis flow meter, (iii) filter was placed upstream of flow meter rather than downstream, and (iv) fluid-to-air heat exchanger was used as condenser instead of fluid-to-water heat exchanger.

2.3. Data processing

Steady state datapoints are obtained by averaging the steady portions of the recorded temporal data and further processed using thermophysical properties from NIST-REFPROP [55]. Fluid enthalpies at the FBM inlet and outlet are determined as

$$h_{in} = h|_{T_{in}, p_{in}} \tag{2}$$

and

$$h_{out} = h_{in} + \frac{q''_w P_h L_h}{\dot{m}}, \tag{3}$$

respectively. Here, T_{in} is FBM inlet fluid temperature, p_{in} FBM inlet pressure, q''_w wall heat flux, $\dot{m}$ mass flow rate, and P_h heated perimeter is equal to channel width, W, for single-sided heating and $2W$ for double-sided heating. These enthalpies are used to determine the corresponding inlet/outlet thermodynamic equilibrium qualities as

$$x_e = \frac{h - h_f\big|_p}{h_{fg}\big|_p}, \tag{4}$$

where both h_f, the saturated liquid enthalpy, and h_{fg}, the latent heat of vaporization, are based on p, the respective measured pressure.

As shown in Fig. 2(c), the FBM's heated section has 7 streamwise wall temperature measurement locations, z = 5.4, 22.7, 40.0, 57.3, 74.6, 91.9, and 109.2 mm, which are designed as 1 upstream through 7 downstream and the corresponding wall temperatures are designated as $T_{wa,z}$, where wa is the heated wall ($w1$ or $w2$). Due to practical limitations, there exists an extended surface area at both ends of the copper strip, which the end resistors must cover. This means the surface heat flux is uniform for the majority

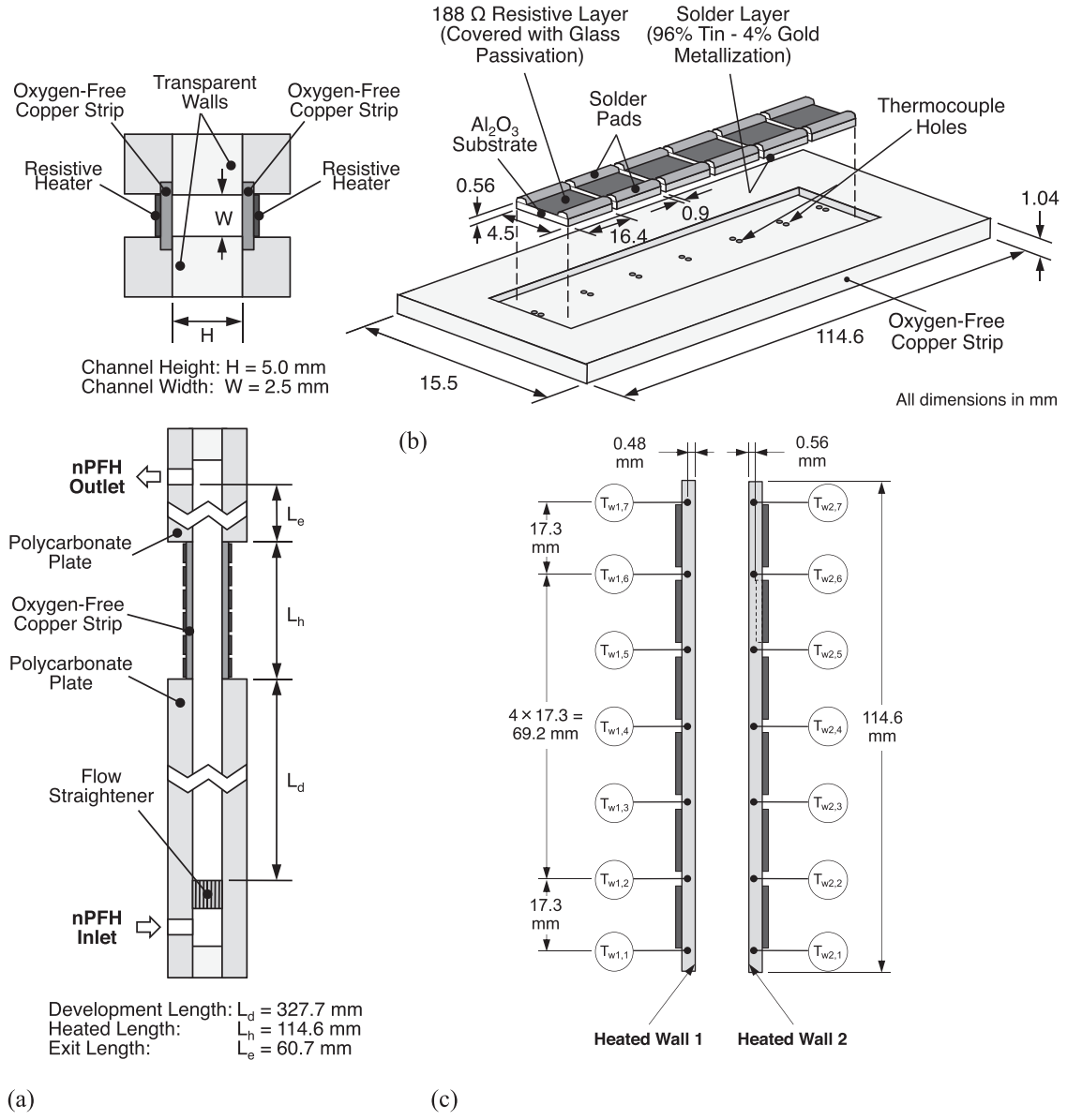

Fig. 2. Schematic representations of (a) overall construction of Flow Boiling Module (FBM), (b) construction of heating strips, and (c) designation of heated walls and wall temperature measurement locations.

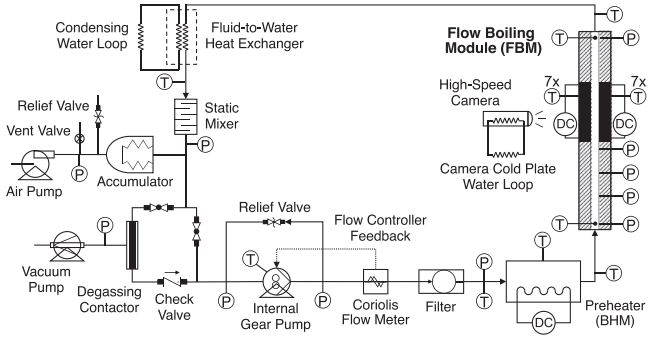

Fig. 3. Schematic diagram of experimental two-phase flow loop used for MST.

of the heated length, except for these extreme locations. To avoid uncertainties, detailed analysis is done in this study for only the middle 5 streamwise locations (2 through 6), while locations 1 and 7 are excluded.

Both local qualities, $x_{e,z}$, and local saturation temperatures, $T_{sat,z}$, at these axial locations are determined by linear interpolation between values at both the inlet and outlet. Local fluid temperatures are determined as

$$T_{f,z} = \begin{cases} T_{in} + (T_{sat,x=0} - T_{in})\frac{z}{L_{h,sp}}, & x_{e,z} < 0 \\ T_{sat,z}, & 0 \le x_{e,z} \le 1, \end{cases} \tag{5}$$

where $L_{h,sp}$ is heated single-phase length defined as

$$L_{h,sp} = \frac{GA_c}{q''_w P_h}\left(h_f\big|_{p_{in}} - h_{in}\right), \tag{6}$$

and $T_{sat,x=0}$ is estimated saturation temperature at the location where $x_e = 0$. Local heat transfer coefficients for either wall is defined as

$$h_{a,z} = \frac{q"_{wa}}{T_{wa,z} - T_{f,z}}. \tag{7}$$

2.4. Experimental cases

Following the authors' prior studies [22,50], the experimental cases in Table 1 are loosely categorized based on inlet subcooling as highly subcooled inlet ($\Delta T_{sub,in}$ > 10°C) and near-saturated inlet ($\Delta T_{sub,in} \leq$ 10°C; close to reaching saturated conditions). It is noted that this subcooling criterion is not derived from physics, but is a rough value based on the present database. Most cases with highly subcooled inlet experience subcooled flow boiling all along the channel, whereas those with near-saturated inlet experience subcooled flow boiling for an upstream length of the channel, which becomes shorter as either heat flux is increased or flow rate decreased. Note that near-saturated inlet comprises both pure subcooled liquid and subcooled liquid-vapor mixture inlet (due to large thermodynamic non-equilibrium coming into the channel), but this aspect is inconsequential for the purposes of this study.

High-speed-video flow visualization images for a representative case of highly subcooled inlet and near-saturated inlet during MST experiments [22] are shown in Figs. 4(a) and 4(b), respectively. The operating conditions are mentioned next to each set of images, and wall heat flux is varied from post-ONB to CHF. Both of them are double-side heated as per the flow schematics shown in Fig. 4(c). Notice how the exit quality, $x_{e,out}$, varies for both, and how the flow features are significantly different for highly subcooled versus near-saturated or saturated boiling. The highly subcooled inlet case in Fig. 4(a) with $\Delta T_{sub,in}$ = 27.49°C has exit qualities ranging up to $x_{e,out}$ = -0.198 near CHF, meaning the fluid is subcooled all along the channel for all heat fluxes. On the other hand, the near-saturated inlet case in Fig. 4(b) with $\Delta T_{sub,in}$ = 7.59°C has subcooled conditions all along the channel for heat fluxes only up to 52.22% q''_{CHF}, whereas at higher heat fluxes, the downstream portion of the channel experiences saturated flow boiling. Moreover, Fig. 4(a) shows the vapor layers along both walls are almost isolated from each other with minimal interaction due to the strongly-condensing liquid core, whereas Fig. 4(b) shows intermingling of vapor layers at the higher heat fluxes where saturated flow boiling is observed. Note that Fig. 4 will also be used for supporting the physics explained in later sections of this study.

2.5. Parametric ranges of consolidated subcooled flow boiling database

Analysis in this study is strictly limited to the subcooled flow boiling regime, *i.e.*, local datapoints where x_e < 0. Additional criteria to remove erroneous datapoints include a positive wall superheat, $T_w > T_{sat}$, and close T_w between the two walls for vertical flows with double-sided heating (for example, this rejected G = 204.39 kg/m^{2}s with vertical downflow for which $T_{w1} >> T_{w2}$ due to possible vapor stagnation near wall 1). Ranges of key parameters of all local subcooled flow boiling datapoints are reported in Table 2 for each subset of the consolidated database.

3. Assessment of prior subcooled flow boiling correlations

3.1. Assessment of seminal correlations

A list of seminal correlations for heat transfer coefficient for subcooled flow boiling are presented in Table 3, along with important remarks on both the database it was developed from and its utilization. Note that some equations are mathematically reformulated for consistency, but the recommendation of the original authors with respect to the choice of both single-phase and pool boiling correlations are adhered to. The present database (combination of working fluid, ranges of operating parameters, partial heating configurations, and various flow orientations in Earth gravity) does not lie within the recommended applicability ranges of the prior

Table 2
Summary of key parameters of consolidated local subcooled flow boiling datapoints.

Dataset	MST (2021) data	MST (2021) data	2016 data	2016 data	2016 data	Overall
Flow orientation	Vertical up	Vertical up	Vertical up	Vertical down	Horizontal	
Heating configuration	Single-sided	Double-sided	Double-sided	Double-sided	Double-sided	
Number of datapoints, N	749	759	353	298	430	2589
Mass flow rate, $\dot{m}$ [g/s]	2.25 – 40.00	2.25 – 40.00	2.16 – 30.49	4.94 – 29.37	2.29 – 30.61	2.16 – 40.00
Mass velocity, G [kg/m^{2}s]	179.93 – 3199.98	180.03 – 3200.00	172.79 – 2438.94	395.39 – 2349.39	182.85 – 2449.19	172.79 – 3200.00
Pressure, p [kPa]	114.54 – 170.52	114.38 – 187.14	109.37 – 228.26	125.12 – 238.44	102.16 – 195.21	102.16 – 238.44
Saturation temperature, T_{sat} [°C]	60.79 – 73.42	60.75 – 76.53	59.36 – 83.19	63.32 – 84.75	57.29 – 77.76	57.29 – 84.75
Fluid temperature, T_f [°C]	35.14 – 72.40	35.56 – 74.12	29.61 – 71.91	30.36 – 72.69	28.30 – 61.83	28.30 – 74.12
Fluid subcooling, ΔT_{sub} [°C]	0.14 – 28.21	0.13 – 27.49	6.23 – 33.27	6.81 – 34.93	10.19 – 31.03	0.13 – 34.93
Quality, x_e	-0.379 – -0.000	-0.369 – -0.001	-0.560 – -0.009	-0.514 – -0.055	-0.486 – -0.065	-0.560 – -0.000
Wall heat flux, q''_w [W/cm^2]	2.08 – 48.09	1.80 – 49.49	4.82 – 49.23	7.23 – 45.66	5.90 – 49.99	1.80 – 49.99
Heated wall temperature, $T_{w,z}$ [°C]	62.10 – 117.38	63.48 – 115.61	59.74 – 106.71	63.57 – 114.15	57.44 – 98.86	57.44 – 117.38
Heat transfer coefficient, h [W/m^{2}K]	1571.26 – 18693.03	1426.28 – 22833.93	2315.79 – 14948.53	3247.30 – 15037.84	2665.44 – 15873.87	1426.28 – 22833.93

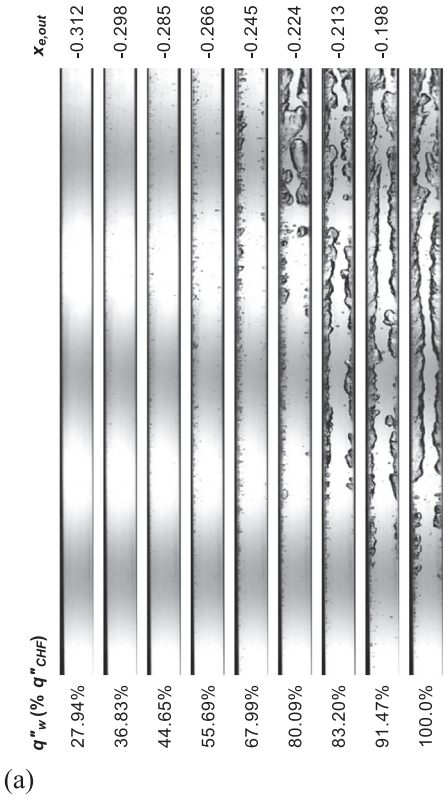

Highly Subcooled Inlet

G = 1599.94 kg/m²s
p_{in} = 124.06 kPa
T_{in} = 35.75°C
$\Delta T_{sub,in}$ = 27.49°C
$x_{e,in}$ = -0.361
q''_{CHF1} = 43.21 W/cm²
q''_{CHF2} = 43.94 W/cm²

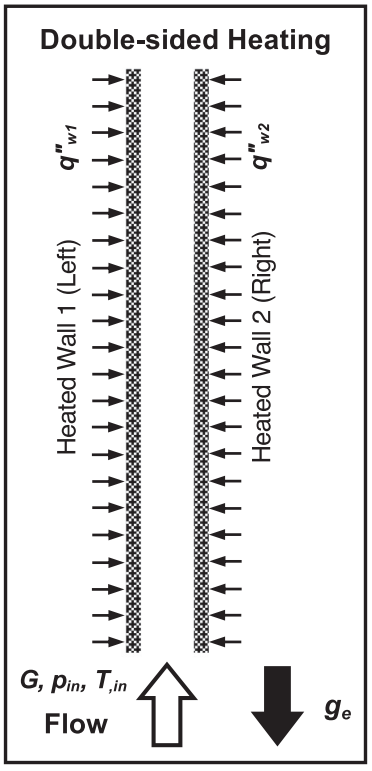

(c)

Near-Saturated Inlet

G = 1599.94 kg/m²s
p_{in} = 148.27 kPa
T_{in} = 61.25°C
$\Delta T_{sub,in}$ = 7.59°C
$x_{e,in}$ = -0.104
q''_{CHF1} = 38.07 W/cm²
q''_{CHF2} = 37.53 W/cm²

Fig. 4. High-speed-video flow visualization images along the boiling curve from post-ONB to CHF for (a) highly subcooled inlet and (b) near-saturated inlet with both walls heated. (c) Schematic representation of double-sided heating configuration.

Table 3
Prior seminal heat transfer coefficient correlations for subcooled flow boiling.

Author(s)	Correlation	Remarks
Papell (1963) [28]	$\frac{Nu_{sc}}{Nu_{sp}} = 90\,(\frac{q''_w}{h_{fg}\rho_g U})^{0.7}(\frac{h_{fg}}{c_{p,f}\Delta T_{sub}})^{0.84}(\frac{\rho_g}{\rho_f})^{0.756}$ $= 90\,Bo^{0.7}Ja^{**-0.84}(\rho_g/\rho_f)^{0.056}$ $Nu_{sp} = 0.021\,\mathrm{Re}_f^{0.8}\,\mathrm{Pr}_f^{0.4}$	• Flow geometry: Uniformly heated tube • Fluids: Distilled water, ammonia • Heated surface: Inconel X • Single-phase heat transfer coefficient is calculated using a Colburn-type equation [66] with properties evaluated at film temperature • Specific heat capacity is estimated at the mean of saturation and bulk fluid temperatures, and all other properties at saturation temperature
Badiuzzaman (1967) [29]	$\frac{Nu_{sc}}{Nu_{sp}} = C_1\,\{(\frac{q''_w}{h_{fg}\rho_g U})(\frac{h_{fg}}{c_{p,f}\Delta T_{sub}})^{1.2}(\frac{\rho_g}{\rho_f})^{1.08}(\frac{\Delta T_{sub}}{T_{sat}})^{0.6}\}^{C_2}$ $= C_1\,\{Bo\,Ja^{**-1.2}(\rho_g/\rho_f)^{0.08}(\Delta T_{sub}/T_{sat})^{0.6}\}^{C_2}$ Water: $C_1 = 178$, $C_2 = 0.75$ Organic fluids: $C_1 = 759$, $C_2 = 0.89$ (used in this study) $Nu_{sp} = 0.021\,\mathrm{Re}_f^{0.8}\,\mathrm{Pr}_f^{0.4}$	• Flow geometry: Over a horizontal rectangular strip • Fluids: Water, ethanol, isopropanol • Heated surface: Stainless steel 321 • Single-phase heat transfer coefficient is calculated using a Colburn-type equation [66] with properties evaluated at film temperature • Specific heat capacity is estimated at the mean of saturation and bulk fluid temperatures, and all other properties at saturation temperature
Moles & Shaw (1972) [31]	$\frac{Nu_{sc}}{Nu_{sp}} = 78.5(\frac{q''_w}{h_{fg}\rho_g U})^{0.67}(\frac{h_{fg}}{c_{p,f}\Delta T_{sub}})^{0.5}(\frac{\rho_g}{\rho_f})^{0.7}(\frac{c_{p,f}\mu_f}{k_f})^{0.46}$ $= 78.5\,Bo^{0.67}Ja^{**-0.5}(\rho_g/\rho_f)^{0.03}\mathrm{Pr}_f^{0.46}$ $Nu_{sp} = 0.027\mathrm{Re}_f^{0.8}\,\mathrm{Pr}_f^{1/3}(\frac{\mu_f}{\mu_f\vert_{T_w}})^{0.14}$	• Flow geometries: Vertical upflow in a circular tube, vertical upflow in rectangular channel, horizontal flow over a heated strip • Fluids: Water, ethanol, isopropanol, n-butanol, ammonia, aniline, hydrazine • Heated surfaces: Stainless steel 347, 304, 321, Inconel X, nickel L and A • Single-phase heat transfer coefficient is calculated using Sieder-Tate equation [58] • Prandtl number is estimated at mean film temperature and all other properties at saturation temperature
Shaw (1972) [32]	$\frac{Nu_{sc}}{Nu_{sp}} = 82(\frac{q''_w}{h_{fg}\rho_g U})^{0.68}(\frac{h_{fg}}{c_{p,f}\Delta T_{sub}})^{0.5}(\frac{\rho_g}{\rho_f})^{0.69}(\frac{c_{p,f}\mu_f}{k_f})^{0.46}$ $= 82\,Bo^{0.68}Ja^{**-0.5}(\rho_g/\rho_f)^{0.01}\mathrm{Pr}_f^{0.46}$ $Nu_{sp} = 0.027\mathrm{Re}_f^{0.8}\,\mathrm{Pr}_f^{1/3}(\frac{\mu_f}{\mu_f\vert_{T_w}})^{0.14}$	• Flow geometries: Vertical upflow in a circular tube, vertical upflow in rectangular channel, horizontal flow over a heated strip, vertically upflow through a channel made of a circular tube placed along the center of a square tube • Fluids: Water, ethanol, isopropanol, n-butanol, ammonia, aniline, hydrazine • Heated surfaces: Stainless steel 304, 321, and 347, Inconel X, nickel L and A • Single-phase heat transfer coefficient is calculated using Sieder-Tate equation [58] • Prandtl number is estimated at mean film temperature and all other properties at saturation temperature
Shah (1977) [37]	$q''_w = h_{sc}(T_w - T_f) = \begin{cases}(\psi_0 + \frac{\Delta T_{sub}}{\Delta T_{sat}})h_{sp}\Delta T_{sat}, & PDB\\ \psi_0 h_{sp}\Delta T_{sat}, & FDB\end{cases}$ $\psi_0 = \begin{cases}230Bo^{0.5}, & Bo > 0.3\times10^{-4}\\ 1+46Bo^{0.5}, & Bo < 0.3\times10^{-4}\end{cases}$ $\frac{h_{sp}D}{k_f} = Nu_{sp} = 0.023\mathrm{Re}_f^{0.8}\mathrm{Pr}_f^{0.4}$	• Flow geometries: Horizontal and vertical tubes, vertical annuli • Fluids: Water, R-113, methanol in annuli; water, R-11, R-12, R-113, methanol, isopropanol, n-butanol, ammonia, aqueous solution of potassium carbonate in other flow geometries • Heated surfaces: Copper, stainless steel, nickel, Inconel, glass • Single-phase heat transfer coefficient is calculated using Dittus-Boelter equation [56,57] • Latent heat is estimated at saturation temperature and all other properties at bulk fluid temperature
Gungor & Winterton (1986) [35]	$q''_w = Eh_{sp}(T_w - T_f) + Sh_{nb}(T_w - T_{sat}) = h_{sc}(T_w - T_f)$ $\Rightarrow h_{sc} = Eh_{sp} + Sh_{nb}\frac{\Delta T_{sat}}{(T_w - T_f)}$ $\frac{h_{sp}D}{k_f} = Nu_{sp} = 0.023\mathrm{Re}_f^{0.8}\mathrm{Pr}_f^{0.4}$ $h_{nb} = 55P_R^{0.12}(-\log_{10}P_R)^{-0.55}M_W^{-0.5}q''^{0.67}_w$ $E = 1;\ S = (1 + 1.15\times10^{-6}E^2\mathrm{Re}_f^{1.17})^{-1}$ For horizontal tubes with $Fr_f \le 0.05$: $E = EFr_f^{0.1-2Fr_f}$ and $S = SFr_f^{0.5}$ $Fr_f = \frac{G^2}{\rho_f^2 gD} = \frac{U^2}{gD}$	• Flow geometries: Vertical and horizontal tubes and annuli • Fluids: Water, refrigerants, ethylene glycol • Single-phase heat transfer coefficient is calculated using Dittus-Boelter equation [56,57] • Nucleate boiling heat transfer coefficient is calculated using Cooper's equation [60]

(*continued on next page*)

Table 3 (*continued*)

Author(s)	Correlation	Remarks
Liu & Winterton (1991) [36]	$q"_w = ((Eh_{sp}(T_w - T_f))^2 + (Sh_{nb}\Delta T_{sat})^2)^{0.5} = h_{sc}(T_w - T_f)$ $\Rightarrow h_{sc} = ((Eh_{sp})^2 + (\frac{Sh_{nb}\Delta T_{sat}}{T_w - T_f})^2)^{0.5}$ $\frac{h_{sp}D}{k_f} = Nu_{sp} = 0.023\mathrm{Re}_f^{0.8}\,\mathrm{Pr}_f^{0.4}$ $E = 1$; $S = (1 + 0.055E^{0.1}\mathrm{Re}_f^{0.16})^{-1} h_{nb} = 55P_R^{0.12}(-\log_{10}(P_R))^{-0.55}M_W^{-0.5}q"_w^{0.67}$ For horizontal tubes with $Fr_f \le 0.05$: $E = EFr_f^{0.1-2Fr_f}$ and $S = SFr_f^{0.5}$	• Flow geometries: Vertical and horizontal tubes and annuli • Fluids: Water, refrigerants, ethylene glycol, ethanol, n-butanol • Single-phase heat transfer coefficient is calculated using Dittus-Boelter equation [56,57] • Nucleate boiling heat transfer coefficient is calculated using Cooper's equation [60] • Liquid Reynolds and Prandtl numbers are estimated at bulk fluid temperature and all other properties at saturation temperature
Shah (2017) [38]	$q''_w = h_{sc}(T_w - T_f) = \begin{cases} \frac{\psi_0 h_{sp}(\Delta T_{sat} - 1.65\Delta T_{sub}^{-0.44})}{0.67}, & PDB \\ \psi_0 h_{sp}\Delta T_{sat}, & FDB \end{cases}$ $\psi_0 = \begin{cases} 230Bo^{0.5}, & Bo > 0.3\times10^{-4} \\ 1 + 46Bo^{0.5}, & Bo < 0.3\times10^{-4} \end{cases}$ $\frac{h_{sp}D}{k_f} = Nu_{sp} = 0.023\mathrm{Re}_f^{0.8}\,\mathrm{Pr}_f^{0.4}$	• Flow geometries: Channels of various geometries and annuli of different heating configurations; horizontal and vertical flows • Fluids: 13 different fluids (water, refrigerants, chemicals) • Heated surfaces: Stainless steel, copper, brass, zirconium-copper alloy, nickel, Inconel, glass • Single-phase heat transfer coefficient is calculated using Dittus-Boelter equation [56,57] • Latent heat is estimated at saturation temperature and all other properties at bulk fluid temperature

correlations. So, the correlations are assessed for their predictive accuracies and, if shown to be good, they can be recommended for use in conditions similar to the present database.

During assessment, the thermophysical properties of nPFH are estimated at the specific temperature or pressure used during the correlation's development and/or recommended in the original study (these are noted in Table 3). The two most popular single-phase *Nu* correlations, Dittus-Boelter [56,57] and Sieder-Tate [58] are used with all properties estimated at the bulk liquid temperature, except for the viscosity denominator in Sieder-Tate which needs to be evaluated at the heated wall temperature. Although the FBM's heated section is relatively short with $L_h/D_h < 60$, the modified version of the Sieder-Tate equation for short channels is not used because the flow is hydrodynamically fully developed at the entrance of the heated section.

The predictive accuracy of each correlation is assessed by a combination of statistical parameters: Mean Absolute Error (MAE), Root Mean Square Error (RMSE), and statistical inliers for ±30% predictive error (ξ_{30}) and ±50% predictive error (ξ_{50}). MAE and RMSE are respectively defined as

$$MAE(\%) = \frac{1}{N}\sum\left|\frac{h_{sc,pred} - h_{sc,exp}}{h_{sc,exp}}\right| \times 100 \tag{8}$$

and

$$RMSE(\%) = \sqrt{\frac{1}{N}\sum\left(\frac{h_{sc,pred} - h_{sc,exp}}{h_{sc,exp}}\right)^2} \times 100. \tag{9}$$

While MAE gives equal weightage to all datapoints while making sure both positive and negative errors do not negate each other, RMSE gives higher weight to outlying errors meaning it will always be larger than MAE and is critical of large errors, and ξ_{30} and ξ_{50} give an exact percentage of datapoints predicted within fixed error magnitudes of 30% and 50%.

3.2. Assessment results and discussion

Parity plots for the assessed seminal correlations are included in Fig. 5, with local datapoints segregated as corresponding to either highly subcooled or near-saturated inlet. The dimensionless-group correlations of Papell [28], Badiuzzaman [29], Moles and Shaw [31], and Shaw [32], respectively shown in Figs. 5(a), (b), (c), and (d), all show a common trend: a '7'-shaped parity plot. The majority of datapoints are predicted almost parallel to the 45° 0%-error line, but there exists some datapoints at the top which are severely overpredicted. These generally-overpredicted datapoints correspond to the nucleate boiling degradation regime between ONBD and CHF, where during experiments, intermittent/partial patches of large coalesced vapor masses on the heated wall reduce heat transfer performance. But this mechanism is not captured in these correlations within any dimensionless group, one reason for which could be due to their experimental databases not containing this region, which in turn could be a consequence of some researchers terminating their flow boiling experiments at ONBD and incorrectly regarding it as true CHF. However, in reality, most forced-convective boiling experiments have an NBD region at heat fluxes close to CHF, where a quasi-steady equilibrium exists between the formation of large coalesced vapor structures on the surface and the flow inertia removing them. True CHF is reached at a point when the incoming flow inertia is no longer strong enough to supply the heated wall with fresh liquid. A similar remark has been made by the authors for jet impingement boiling with further details and experimental recommendations [10,59]. Flow visualization images from the present experiments (for example, see Fig. 4) corroborate this mechanism, where close to CHF, almost the entire heated walls are insulated with a wavy vapor layer with small troughs (termed *wetting fronts*) supplying liquid for nucleate boiling, and CHF is reached when these wetting fronts are extinguished [22,50]. The second reason for these overpredictions is these correlations have a ΔT_{sub} parameter raised to a negative power, which worsens predictions as $x_e \to 0$.

Papell's [28] correlation performs poorly for all datapoints with a MAE of 56.45% because even the 45° cluster of data lies below the -30%-error prediction line. This could be due to nPFH having significantly different thermophysical properties compared to water and ammonia, the only fluids in their database. Badiuzzaman's [29] correlation has a major uncertainty in its form; the original article was prepared using Imperial units and it specifically states that the unit of all temperatures is °F (and no mention of the Rankine scale). This is important for one dimensionless group, their newly-introduced temperature ratio. Using °F, the

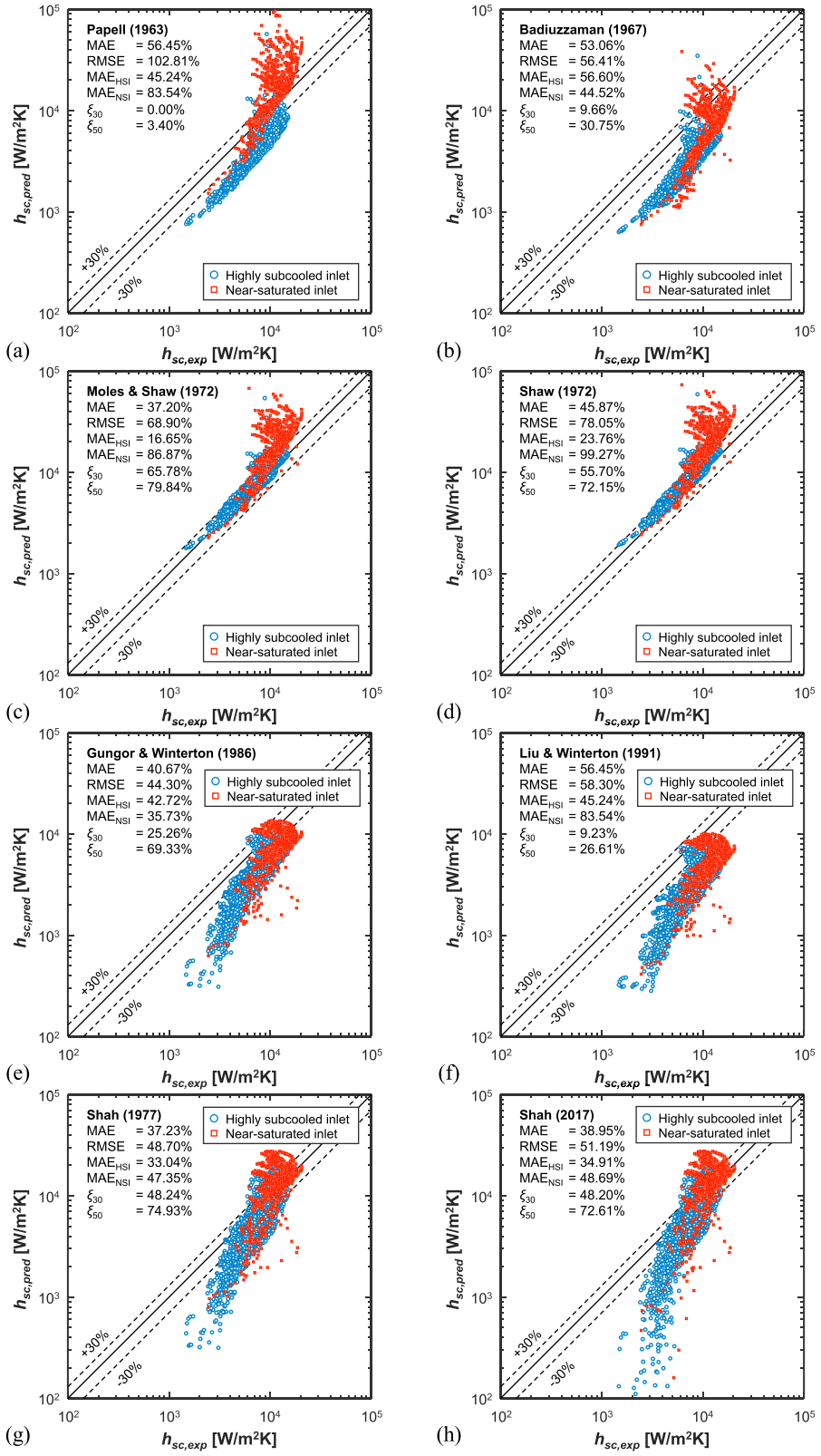

Fig. 5. Parity plots assessing the predictive performance of prior seminal correlations: (a) Papell [28], (b) Badiuzzaman [29], (c) Moles and Shaw [31], (d) Shaw [32], (e) Gungor and Winterton [35], (f) Liu and Winterton [36], (g) Shah [37], and (h) Shah [38].

MAE is very high at 129.25%. Since this is physically incorrect, Fig. 5(b) shows the results obtained using Kelvin (equivalent to Rankine; both are absolute temperature scales). Again, the trends are similar to Papell's, but with the highly subcooled datapoints more underpredicted and the near-saturated-inlet datapoints better predicted. Surprisingly, when the temperature ratio is based on °C (again non-physical), the predictions are good with a MAE of 34.08%. Moles and Shaw's [31] correlation is by far the most accurate correlation for the present database with an overall MAE of 37.20% and ξ_{30} = 65.78%. Most datapoints fall within the ±30%-error band, with only the near-saturated datapoints worsening the prediction results. Shaw [32] later conducted experiments of subcooled boiling in an annulus-like geometry, added these results to their consolidated database, and proposed new empirical constants to their former correlation. It yields similar trends with an upwards shift of all datapoints, overpredicting and worsening the MAE to 45.87%.

The superposition-type correlations of both Gungor and Winterton [35] and Liu and Winterton [36] yield large MAEs of 40.67% and 56.45% as shown in Figs. 5(e) and 5(f), respectively. Both are based on Chen's [33] correlation for saturated flow boiling and use the same auxiliary correlations for liquid convection (Dittus-Boelter) and nucleate pool boiling (Cooper [60]), but with modified enhancement and suppression factors. Gungor and Winterton did a weighted-summation of the two terms, whereas Liu and Winterton used a weighted root mean square. For subcooled flow boiling, they used the same enhancement factor of unity but different empirically-derived suppression factors. Although both of these correlations are based on consolidated databases containing a variety of fluids flowing in both vertical and horizontal orientations, they yield mostly underpredicted values with only a small subset of datapoints within the ±30%-error band.

Shah proposed his first empirical correlation for subcooled flow boiling in 1977 [37], which requires the demarcation of datapoints into PDB and FDB based on his own empirically-derived criterion. As shown in Fig. 5(g), the predictions are almost acceptable with a MAE of 37.23%, but the cluster of datapoints are at an angle larger than 45°, which could be the cause of improperly-tuned empirical constants for the present study. Shah later modified his correlation in 2017 [38], by broadening his consolidated database. However, as shown in Fig. 5(h), this barely changed the predictions, evident from a MAE of 38.95%.

3.3. Inspection of Moles and Shaw's correlation

The best performing seminal correlation for the present database, Moles and Shaw's, is inspected further. This same correlation also yielded the best predictions for subcooled flow boiling of both HFE-7100 in conventional-sized annuli [7] and R-134a in parallel micro-channel array heat sinks [61]. This means that the dimensionless groups considered in this correlation's formulation accurately considers the physical mechanisms in subcooled flow boiling, at least for PDB and FDB. Fig. 6 shows a plot of $h_{sc,pred}/h_{sc,exp}$ versus local quality, where the majority of datapoints are predicted within the ±30%-error band, with almost no underpredictions. Some overpredictions of < 100% are present in the range of -0.36 < x_e < -0.00 and are indicative of the NBD regime. The huge overpredictions in the range of -0.10 < x_e < -0.00 are due to the bad form of the correlation itself; in fact, this is a major drawback of the dimensionless-group-type correlations proposed so far. Inverse of the Jacob number term produces an artificial singularity at ΔT_{sub} = 0. The MAEs for each subset of x_e are seen to worsen as flow reaches saturation. Note that a workaround based on purely mathematical extrapolation was previously suggested by the present authors in [21], but this is avoidable if the correlation form itself can be modified.

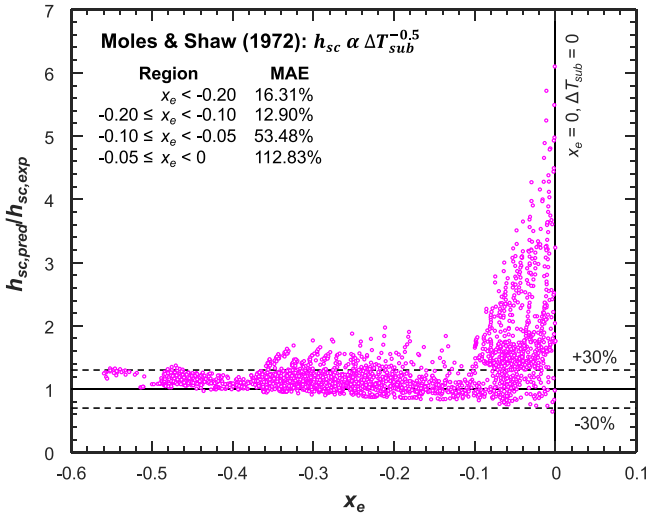

Fig. 6. $h_{sc,pred}/h_{sc,exp}$ ratio versus thermodynamic equilibrium quality for Moles and Shaw's [31] correlation.

4. Development of new subcooled flow boiling correlation

4.1. Development rationale

From both Section 3 and prior literature, it is clear that correlations based on dimensionless groups provide the overall best predictions for both PDB and FDB, perform better, and are easily usable compared to superposition-type correlations (some of which are implicit equations and need iterations). Especially, the correlation by Moles and Shaw [31] yields very good predictions for the highly subcooled boiling regime, but suffers from a serious drawback due to its functional form itself (refer to section 3.3 for details). This method is pursued to develop a new correlation in this study, but by carefully selecting a functional form to avoid artificial singularities within its range of applicability, and to provide reliable predictions befitting both experimentally-observed flow physics and trends shown in past correlations. Before proceeding, the boiling curves in the consolidated database are analyzed and information extracted.

4.2. Flow boiling curves for different flow orientations in Earth gravity

The different flow orientations in Earth gravity are shown in Fig. 7 along with the corresponding wall angles, where vertical upflow (θ = 90°), vertical downflow (θ = -90°), and horizontal flow (θ = 0°, 180°) are the primary ones; all other intermediate orientations are expected to yield results between those of the primary ones. Due to both vertical flow orientations being parallel to gravity, the two walls are expected to yield similar boiling behavior and do not need differentiation, provided both cavity distribution and heat flux are identical for both. On the other hand, horizontal flows need differentiation between the two walls due to buoyancy acting perpendicular to flow, hence each wall is denoted by a different angle. Examples of flow boiling curves for each orientation and heating configuration are presented in this section along with identification of the fully developed nucleate boiling region for each wall (similar to the schematic curve in Fig. 1).

4.2.1. Vertical upflow with single-sided heating

Boiling curves for vertical upflow with single-sided heating and near-saturated inlet are shown in Fig. 8 for streamwise locations of z = 22.7, 40.0, 57.3, 74.6, and 91.9 mm from inlet of heated

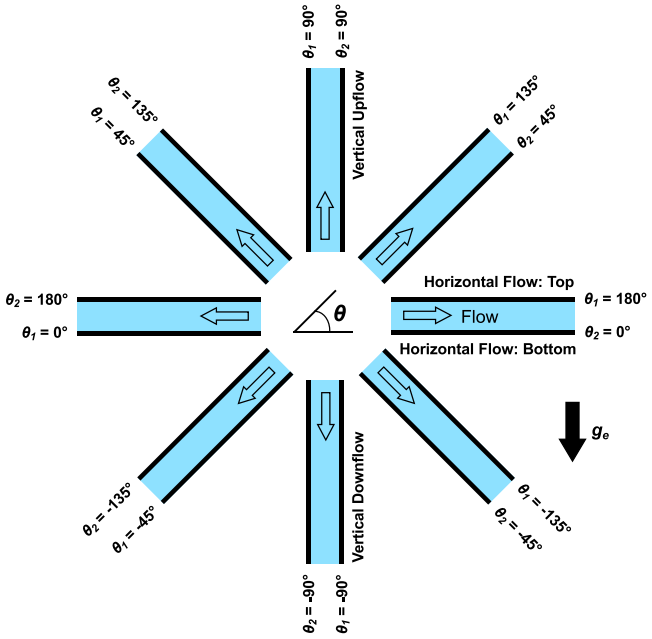

Fig. 7. Schematics of different flow orientations with respect to gravity and the corresponding wall angles.

section. Ranges of operating conditions for these curves are presented within the figure; the parameter which varies the most is inlet pressure, which increases as heat flux is increased due to increased flow resistance when more vapor is generated. However, this effect is isolated from the curves by subtracting inlet saturation temperature from the wall temperature on the horizontal axis. As explained in Section 1.3, the almost linear portion of the curve represents the fully developed nucleate boiling regime; this is indicated by the linear tangents drawn for each curve. The lower point of intersection represents transition from PDB to FDB and the upper point of transition represents ONBD. At the most upstream location of $z = 22.7$ mm, both ONBD and PDB-FDB transition occur at higher heat fluxes and the majority of the boiling curve is dominated by fully developed nucleate boiling. As we move downstream, although the PDB-FDB-transition heat flux does not change by much, q''_{ONBD} decreases significantly to a point where, at $z = 91.9$ mm, $q''_{ONBD} \approx 16$ W/cm^2 and the upper half of the curve experiences NBD. The other notable behavior is the slope of the FDB tangent increases as we move downstream. Note that due to the small inlet subcooling, flow transitions from subcooled boiling to saturated boiling at a certain downstream location, which moves upstream as heat flux is increased.

4.2.2. Vertical upflow with double-sided heating

Similar boiling curves for vertical upflow with double-sided heating and highly subcooled inlet are shown in Fig. 9. At $z = 22.7$ and 74.6 mm, the FDB tangents for both walls overlap, whereas a slight difference in slopes exist at the other locations. This can be attributed to preferential bubble production although both walls are polished to the same grade. Trends of NBD are much more obvious for these operating conditions with negligible degradation at $z = 22.7$ mm for all heat fluxes and degradation becoming rather significant and enormous as we move downstream. This can be seen from the difference in wall superheats at ONBD and

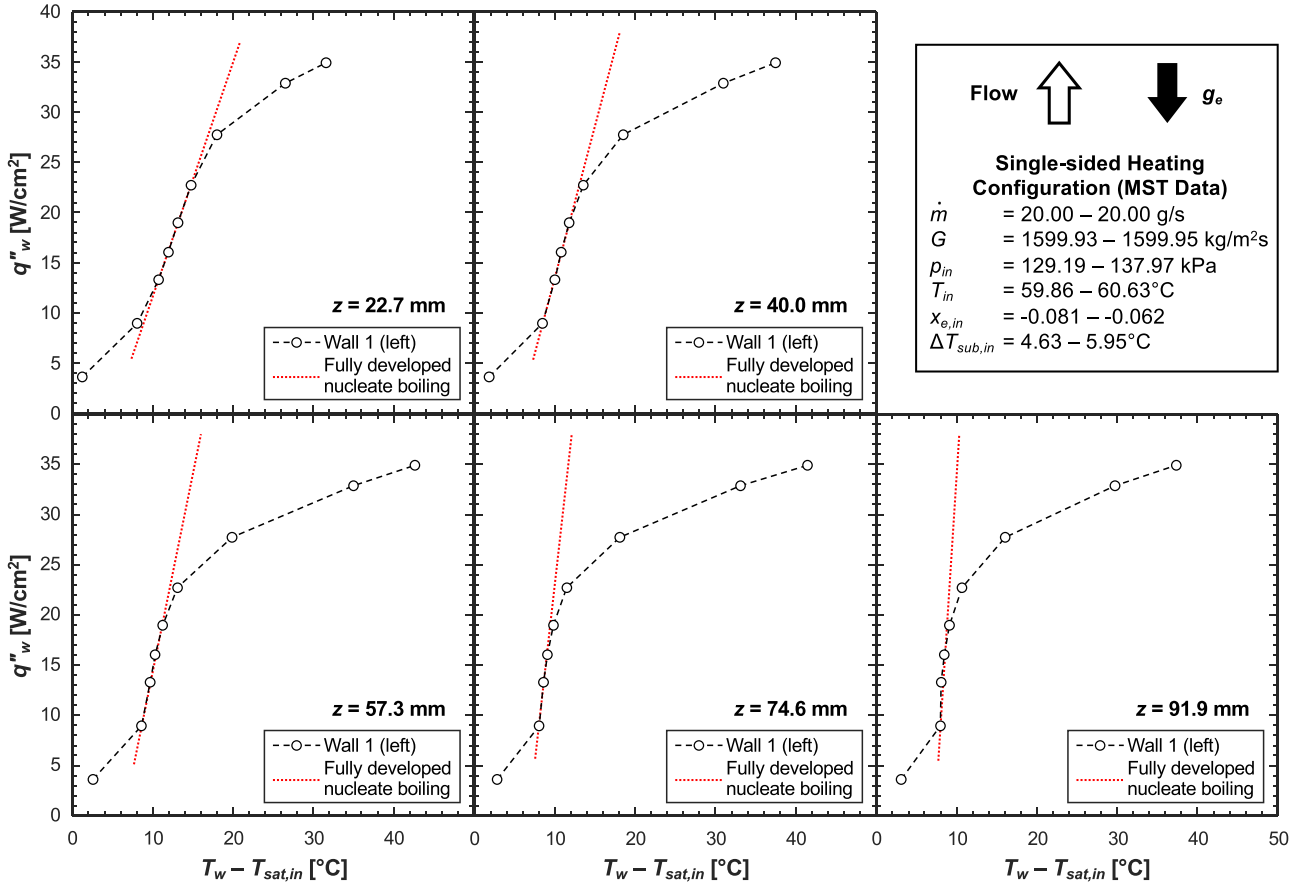

Fig. 8. Flow boiling curves for vertical upflow with single-sided heating and near-saturated inlet at locations of $z = 22.7$, 40.0, 57.3, 74.6, and 91.9 mm from inlet of heated section. Fully developed nucleate boiling region of each curve is shown.

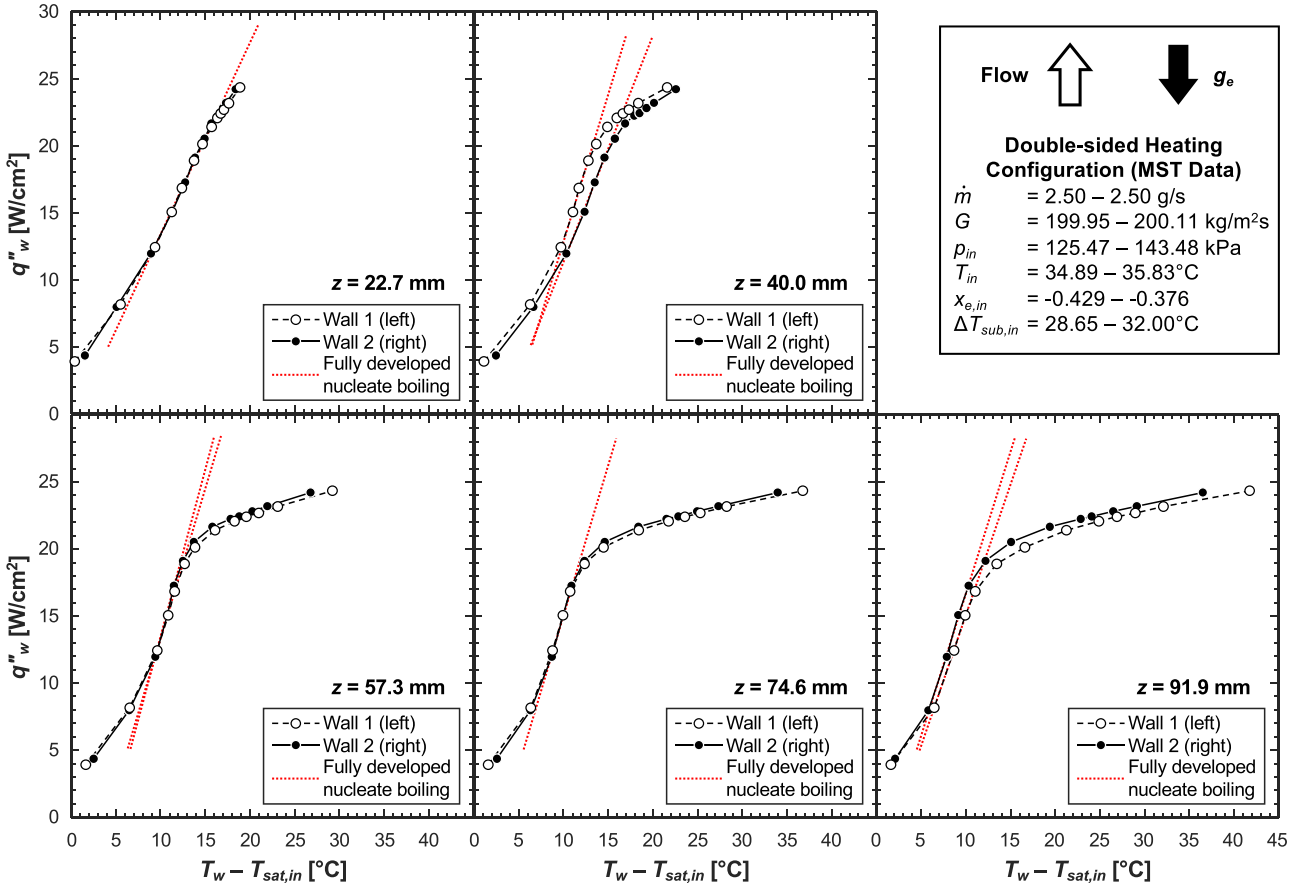

Fig. 9. Flow boiling curves for vertical upflow with double-sided heating and highly subcooled inlet at locations of z = 22.7, 40.0, 57.3, 74.6, and 91.9 mm from inlet of heated section. Fully developed nucleate boiling region of each curve is shown.

CHF gradually increasing as flow moves downstream. At z = 91.9 mm, T_{w1} increases by 31°C for a 7.5-W/cm^2 increase in q''_{w1}, which shows the significance of NBD.

4.2.3. Vertical downflow with double-sided heating

Similar boiling curves are shown in Fig. 10 for vertical downflow with double-sided heating and highly subcooled inlet. The trends are similar to vertical upflow, however both q''_{ONBD} and q''_{CHF} are smaller than upflow due to vapor stagnation in the channel causing NBD at much lower heat fluxes. For these experiments, the two walls had slight differences in supplied heat flux, which caused the two curves to be farther apart in the degraded region although the PDB and FDB regions overlap.

4.2.4. Horizontal flow with double-sided heating

Fig. 11 contains boiling curves for five streamwise locations of horizonal flow with double-sided heating and highly subcooled inlet. At all locations, the lower portions of the curves for both walls are almost identical to each other meaning gravity has negligible influence on the transition from PDB to FDB. But the upper portions of the boiling curves follow a different trend: the top wall's curves have ONBD at a much lower heat flux, leading to CHF. This is due to flow stratification with the generated vapor accumulating under the top wall reducing fresh liquid access for nucleate boiling. On the other hand, the bottom wall does not experience NBD until z = 57.3 mm even when the top wall experiences CHF. Even at the most downstream location of z = 91.9 mm, as evident from the wall temperatures, the bottom wall experiences NBD to a lesser extent than the top wall. This means that, as opposed to vertical flows, the top and bottom walls in horizontal flow need to be considered independently for heat transfer analysis.

Similar analysis is manually done for all boiling curves (except for those having lesser than six heat flux increments) considered in this study (see Table 1) and the FDB datapoints are extracted from the consolidated local h database. The datapoints below and above FDB in each curve belong to PDB and NBD, respectively. The authors believe that this would be more accurate than using an empirical criterion for PDB-FDB transition from the literature (*e.g.*, Shah [37]), and ONBD criteria for subcooled boiling are rare in the literature. Furthermore, since this was not the focus of these experiments, the heat flux increments are large until near CHF, meaning errors associated with isolating these PDB-FDB transition and ONBD points are large. So, relations for these are not pursued at this time. The well-identifiable and reliable FDB regime datapoints, a summary of which is shown in the first column of Table 4, are considered for further analysis. Summaries of PDB and NBD datapoints are included in the second and third columns of Table 4.

4.3. Formulation of correlation for fully developed subcooled flow boiling

From both dimensional analysis [32] and analysis of prior correlations, Nusselt number ratio (equivalent to the heat transfer enhancement provided by subcooled boiling over pure liquid convection), Nu_{sc}/Nu_{sp}, is expected to have the following functional form,

$$\frac{Nu_{sc}}{Nu_{sp}} = \frac{h_{sc}}{h_{sp}} = f\left\{\frac{q''_w}{Gh_{fg}}, \frac{\rho_g}{\rho_f}, \frac{c_{p,f}\Delta T_{sub}}{h_{fg}}, \frac{c_{p,f}\mu_f}{k_f}, \ldots\right\}, \tag{10}$$

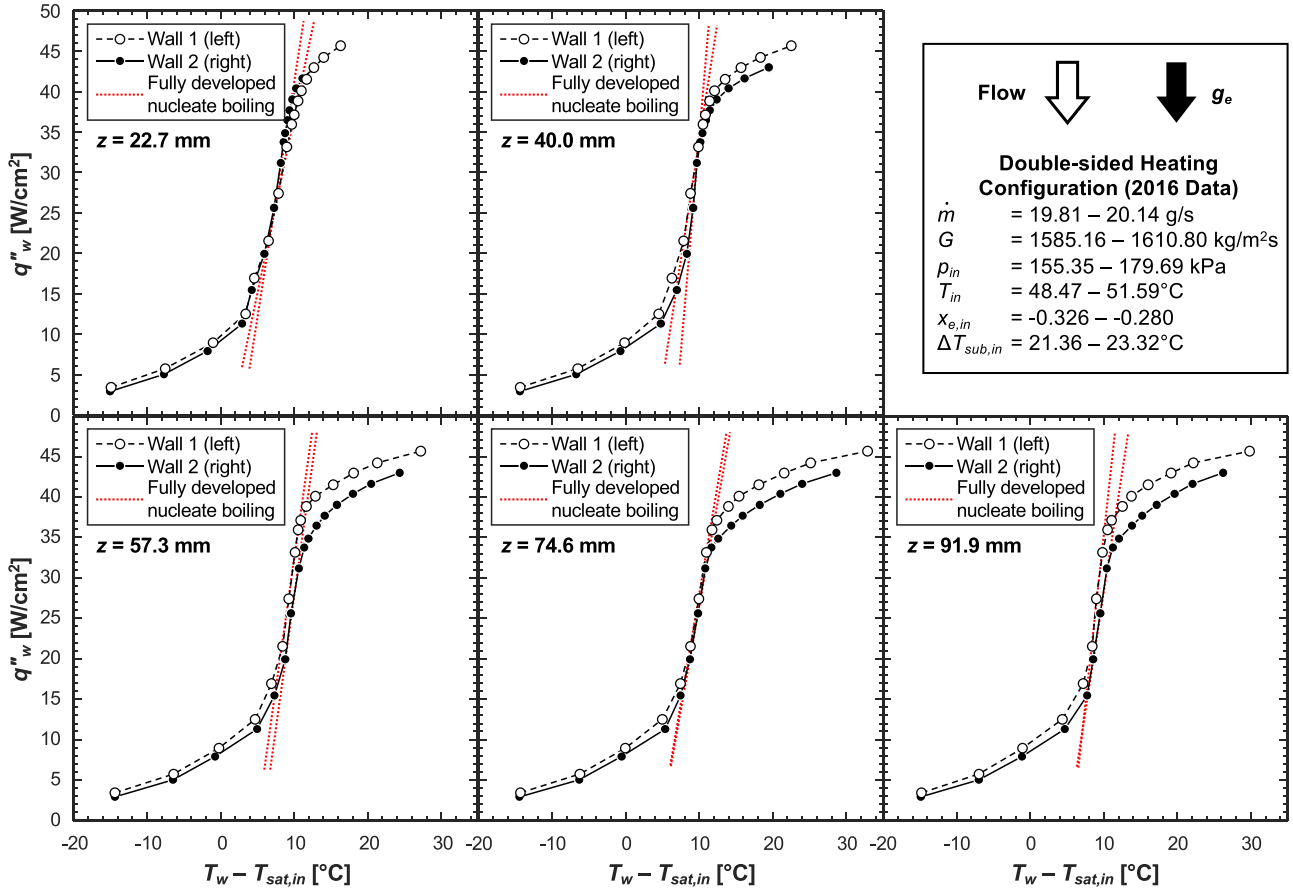

Fig. 10. Flow boiling curves for vertical downflow with double-sided heating and highly subcooled inlet at locations of z = 22.7, 40.0, 57.3, 74.6, and 91.9 mm from inlet of heated section. Fully developed nucleate boiling region of each curve is shown.

Table 4
Summary of demarcated local subcooled flow boiling datapoints.

	FDB	PDB	NBD
Flow orientations (θ)	Vertical up (90°), Vertical down (-90°), Horizontal (0°, 180°)		
Heating configurations	Single-sided and double-sided heating of rectangular channel		
Number of datapoints, N	1275	812	922
Mass velocity, G [kg/m^{2}s]	175.30 – 3199.99	172.79 – 3199.98	179.99 – 3200.00
Pressure, p [kPa]	103.28 – 225.56	102.16 – 203.70	113.01 – 238.44
Saturation temperature, T_{sat} [°C]	57.62 – 82.77	57.29 – 79.38	60.34 – 84.75
Fluid temperature, T_f [°C]	29.08 – 72.77	28.30 – 72.79	33.25 – 74.12
Fluid subcooling, ΔT_{sub} [°C]	0.28 – 34.93	0.13 – 33.27	0.23 – 30.66
Quality, x_e	-0.556 – -0.001	-0.558 – 0.000	-0.479 – 0.001
Wall heat flux, q''_w [W/cm^2]	3.80 – 48.27	2.05 – 35.76	8.39 – 49.99
Reduced pressure, p/p_{crit}	0.059 – 0.130	0.059 – 0.117	0.065 – 0.137
Boiling number, Bo	$(5.203 – 175.8) \times 10^{-4}$	$(1.647 – 102.5) \times 10^{-4}$	$(11.17 – 187.6) \times 10^{-4}$
Modified Jacob number, Ja^{**}	0.004 – 0.474	0.002 – 0.461	0.003 – 0.413
Reynolds number, Re_{fo}	966.72 – 26043.83	1020.53 – 25830.14	1250.70 – 26883.66
Prandtl number, Pr_f	5.76 – 7.38	5.95 – 7.40	5.65 – 7.18
Density ratio, ρ_f/ρ_g	51.38 – 116.35	57.33 – 117.66	48.38 – 106.11

where all thermophysical properties are estimated based on local pressure (*i.e.*, local saturation temperature). For simplicity in use, an explicit correlation for single-phase Nusselt number of turbulent flows, the Dittus-Boelter correlation,

$$Nu_{sp} = \frac{h_{sp}D_h}{k_f} = 0.023\mathrm{Re}_{fo}^{0.8}Pr_f^{0.4}, \tag{11}$$

is selected, where all properties are based on the local bulk fluid temperature (as per the development of the original correlation) and liquid-only Reynolds number is based on hydraulic diameter.

Non-linear regression is performed in MATLAB software with a bisquare tuning constant of 4.685 [62] to determine the empirical constants and the statistical significance of each group in the functional form. Hypothesis testing is a statistical inference technique used to extract information from an available database to assess the validity of either the null or alternative hypotheses. Null hypothesis is valid when there is absolutely no relation of one parameter on another, whereas the alternative hypothesis is valid when some dependence can be established. The probability value, p-value, is defined as the largest probability that datapoints from any other database will be equal to the values predicted by the

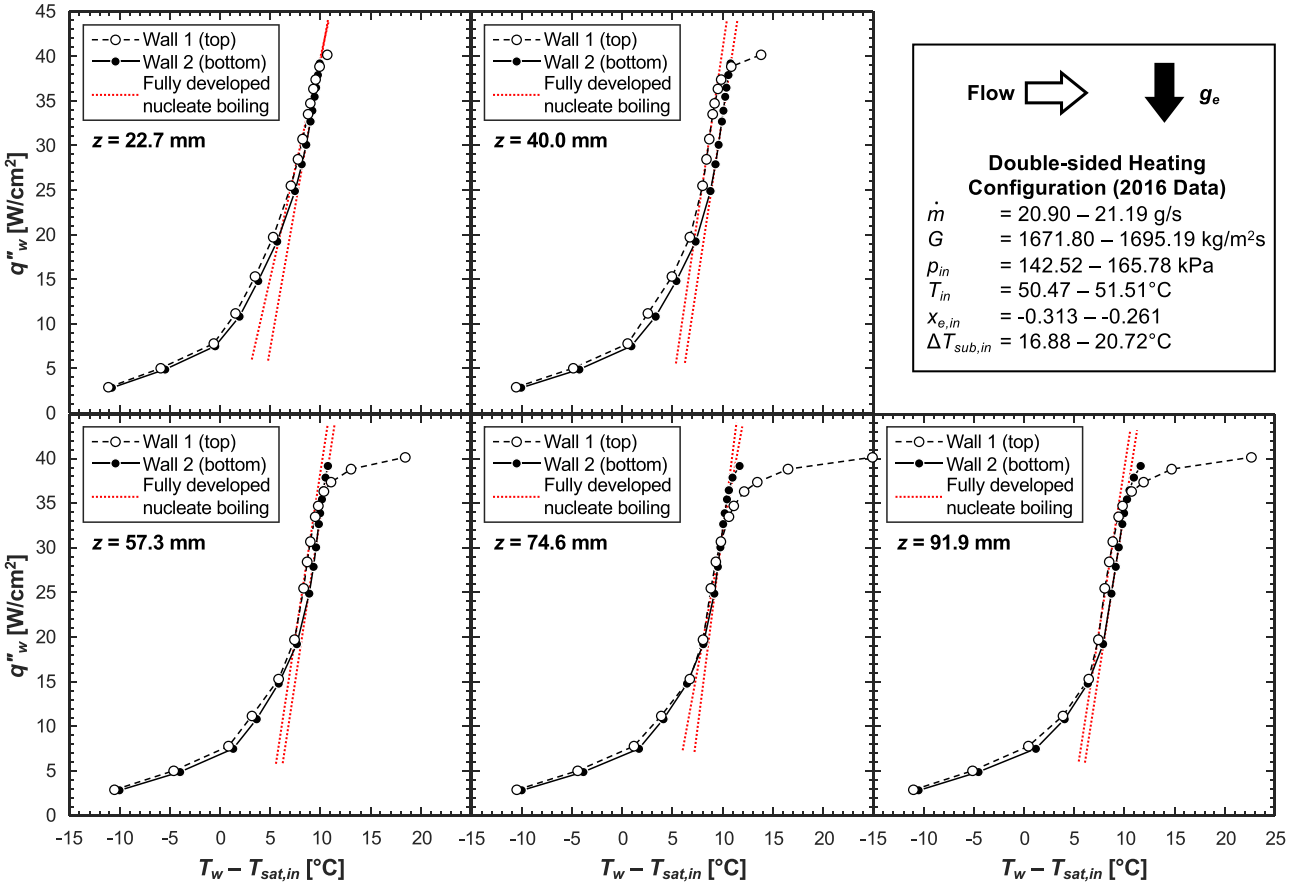

Fig. 11. Flow boiling curves for horizontal flow with double-sided heating and highly subcooled inlet at locations of z = 22.7, 40.0, 57.3, 74.6, and 91.9 mm from inlet of heated section. Fully developed nucleate boiling region of each curve is shown.

present correlation model, assuming the null hypothesis is true and the chosen model valid. Null hypothesis is considered true by default, but if p-value $\leq$ 0.05 (equivalent to a 5% significance level of that parameter), it can usually be rejected [10,63]. p-values are usually $>$ 0.05 if the selected dimensionless group has no effect on h_{sc}/h_{sp}, or if it is redundant (*i.e.*, its effects are already accounted for by another group or combinations of several groups).

Boiling number and modified Jacob number, the two terms that mostly affect heat transfer enhancement and are consistent in all seminal dimensionless-group correlations, are preserved. For the present database used for regression (FDB in Table 4), modified Jacob number varies in the range of $0.039 \leq Ja^{**} \leq 0.474$, and to remove the singularity as $\Delta T_{sub} \rightarrow 0$, $(0.1 + Ja^{**})$ is used instead of Ja^{**}. A value of 0.1 ensures that the added constant does not overshadow the effects of subcooling and preserves physical trends.

Upon checking the significance of each dimensionless group on h_{sc}/h_{sp}, it is deemed both vapor-to-liquid density ratio and liquid Prandtl number do not have any significant effect for the parametric ranges of the present database with just one fluid, nPFH. In fact, preliminary correlations made with or without these terms yielded almost the same trends and errors in prediction. Hence, these two terms are merged with the leading constant in the final form,

$$\frac{h_{sc}}{h_{sp}} = C_1 \left(\frac{q"_w}{G h_{fg}} \right)^{C_2} \left(0.1 + \frac{c_{p,f} \Delta T_{sub}}{h_{fg}} \right)^{C_3}. \tag{12}$$

In Eq. (12), terms conveying the channel heating configuration are absent, due to both a statistical insignificance of such terms on h_{sc}/h_{sp} and the flow physics. Let us carefully assess the flow visualization images shown in Figs. 4(a) and 4(b), respectively, for representative cases of highly subcooled inlet and near-saturated inlet. In Fig. 4(a), for all heat fluxes, highly subcooled boiling with double-sided heating clearly results in less interaction between the bubbles and coalesced vapor structures produced at both walls. Moreover, the increased streamwise flow acceleration for double-side heating is insignificant due to both strong condensation simultaneously occurring and latent heat domination during FDB. In Fig. 4(b), near-saturated conditions do show a similar behavior only at lower heat fluxes. Thus, in subcooled flow boiling, heat transfer is insignificantly affected by the number of channel walls heated due to the large condensing capability of the bulk fluid. However, during saturated flow boiling, one must expect (i) more significant interactions between the bubble boundary and/or vapor layers at both walls and (ii) the produced vapor accelerating the flow resulting in increased heat transfer. As a result, saturated h correlations often use heated-to-friction perimeter ratios [64] or other equivalent diameters in their development. Furthermore, terms containing flow orientation ended up not being needed due to orientation insignificantly affecting fully developed subcooled flow boiling.

4.4. New correlation and its statistics

The final correlation is

$$\frac{h_{sc}}{h_{sp}} = 312.8 \left(\frac{q"_w}{G h_{fg}} \right)^{0.769} \left(0.1 + \frac{c_{p,f} \Delta T_{sub}}{h_{fg}} \right)^{-0.632}$$

$$\Rightarrow \frac{Nu_{sc}}{Nu_{sp}} = 312.8 Bo^{0.769} (0.1 + Ja^{**})^{-0.632}, \tag{13}$$

where the constants are regressed with an aim of minimizing the predictive error (the numerical regression is made sure to find the

Table 5
Prediction statistics for the new correlation for fully developed subcooled flow boiling regime (development database).

Flow orientation	Heating configuration (dataset)	*N*	*MAE*	*RMSE*	ξ_{15}	ξ_{30}
Vertical upflow	Single-sided (MST)	259	7.01%	9.62%	91.89%	98.07%
	Double-sided (MST)	258	10.19%	12.34%	76.74%	98.84%
	Double-sided (2016)	173	5.97%	7.40%	94.22%	100.0%
Vertical downflow	Double-sided (2016)	147	4.36%	5.29%	100.0%	100.0%
Horizontal flow	Double-sided: Top wall (2016)	204	5.69%	6.86%	99.02%	100.0%
	Double-sided: Bottom wall (2016)	234	6.52%	8.21%	92.31%	100.0%
Overall		**1275**	**6.91%**	**8.95%**	**91.29%**	**99.37%**

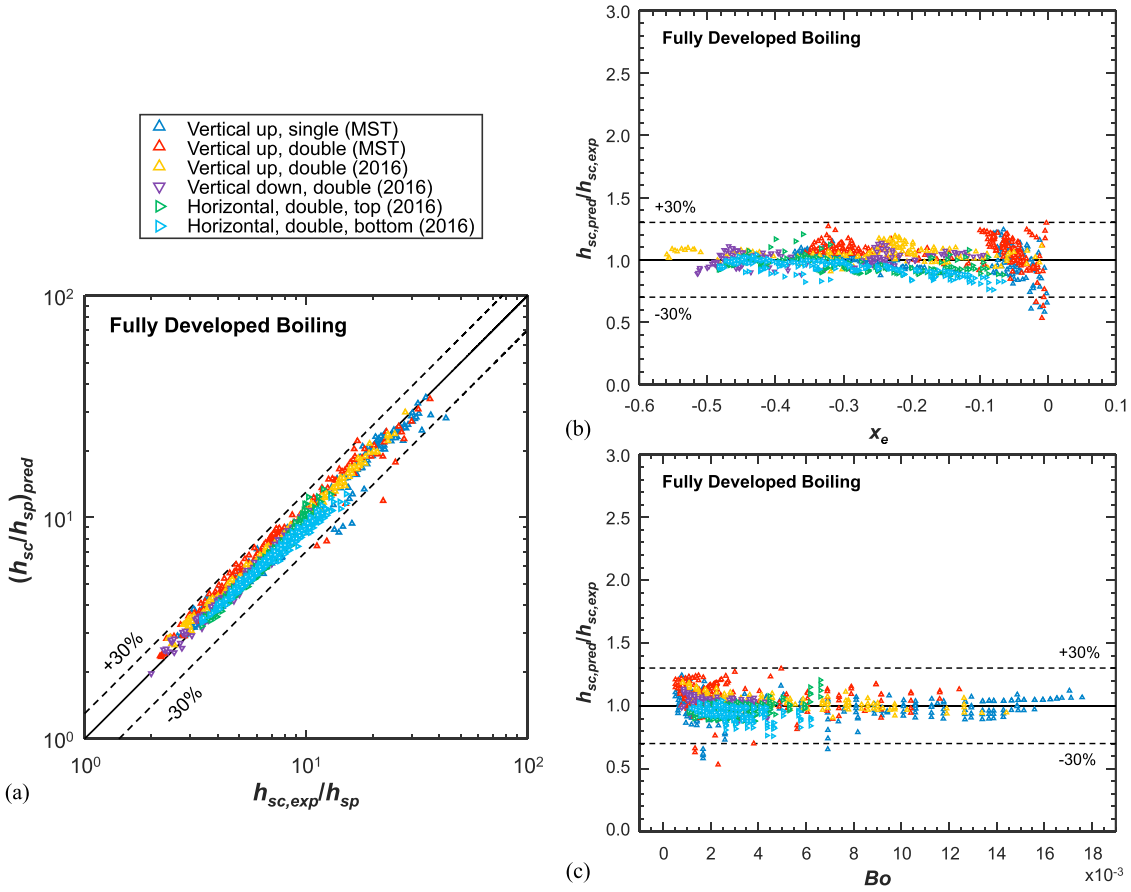

Fig. 12. Prediction trends of new correlation for fully developed boiling regime: (a) Predicted versus experimental h_{sc}/h_{sp} ratio (enhancement factor), (b) $h_{sc,pred}/h_{sc,exp}$ versus thermodynamic equilibrium quality, and (c) $h_{sc,pred}/h_{sc,exp}$ versus boiling number. Data markers are segregated for different subsets of the consolidated database.

global minima within the expected ranges), while preserving physical trends. A maximum standard error of 1.21% is associated with the leading constant, and all constants have a p-value of zero, rejecting the null hypothesis for all parameters and proving the validity of the chosen correlation form. The exponent on *Bo*, 0.769, is in the same range as seen in seminal correlations (Papell: 0.7 [28], Badiuzzaman: 0.75, 0.89 [29], Moles and Shaw: 0.67 [31]; see Table 3). Even with the addition of a constant to Ja^{**}, which changes the nature of the curve, its exponent of -0.632, falls among the significantly-different exponents used for just Ja^{**} in prior correlations (Papell: -0.84, Badiuzzman: -0.9, -1.07, Moles and Shaw: -0.5).

Its predictive performance over the entire FDB database (first column in Table 4) is shown both statistically in Table 5 and figuratively in Fig. 12. An overall MAE of 6.91% reflects the excellent predictive capability and an overall RMSE of 8.95%, which is very close to the MAE, indicates that the spread of the prediction errors is small and the outlying errors are very few. In the parity plot of $(h_{sc,pred}/h_{sp})$ versus $(h_{sc,exp}/h_{sp})$ in Fig. 12(a), excepting 8 stray datapoints, the entire database falls within the ±30%-error band, also evident by ξ_{30} = 99.37%. In fact, 91.29% of the database is predicted within ±15% error. Furthermore, the new correlation yields good predictions for each subset of the database, with the largest errors seen for vertical-upflow MST data. This is because only the MST dataset includes near-saturated inlet data, which (i) experienced severe thermodynamic non-equilibrium even before boiling started within the FBM [22], and is inherently sensitive to (ii) measurement uncertainties (for instance, thermocouples have a maximum uncertainty of ±0.5°C and pressure transducers ±0.7 kPa [22], meaning uncertainties in T_f is ~±0.5°C, T_{sat} is ~±(0.3+0.3)°C, and ΔT_{sub} is ~±1.1°C, so the estimation of very low local subcoolings < ~5°C is associated with a large uncertainty) and (iii) assumptions made during data processing (for example, the estimation of local pressure by linear interpolation between values measured at the inlet and outlet). Fig. 12(b) shows $(h_{sc,pred}/h_{sc,exp})$ ratio versus x_e, and confirms that (i) the new correlation has a uni-

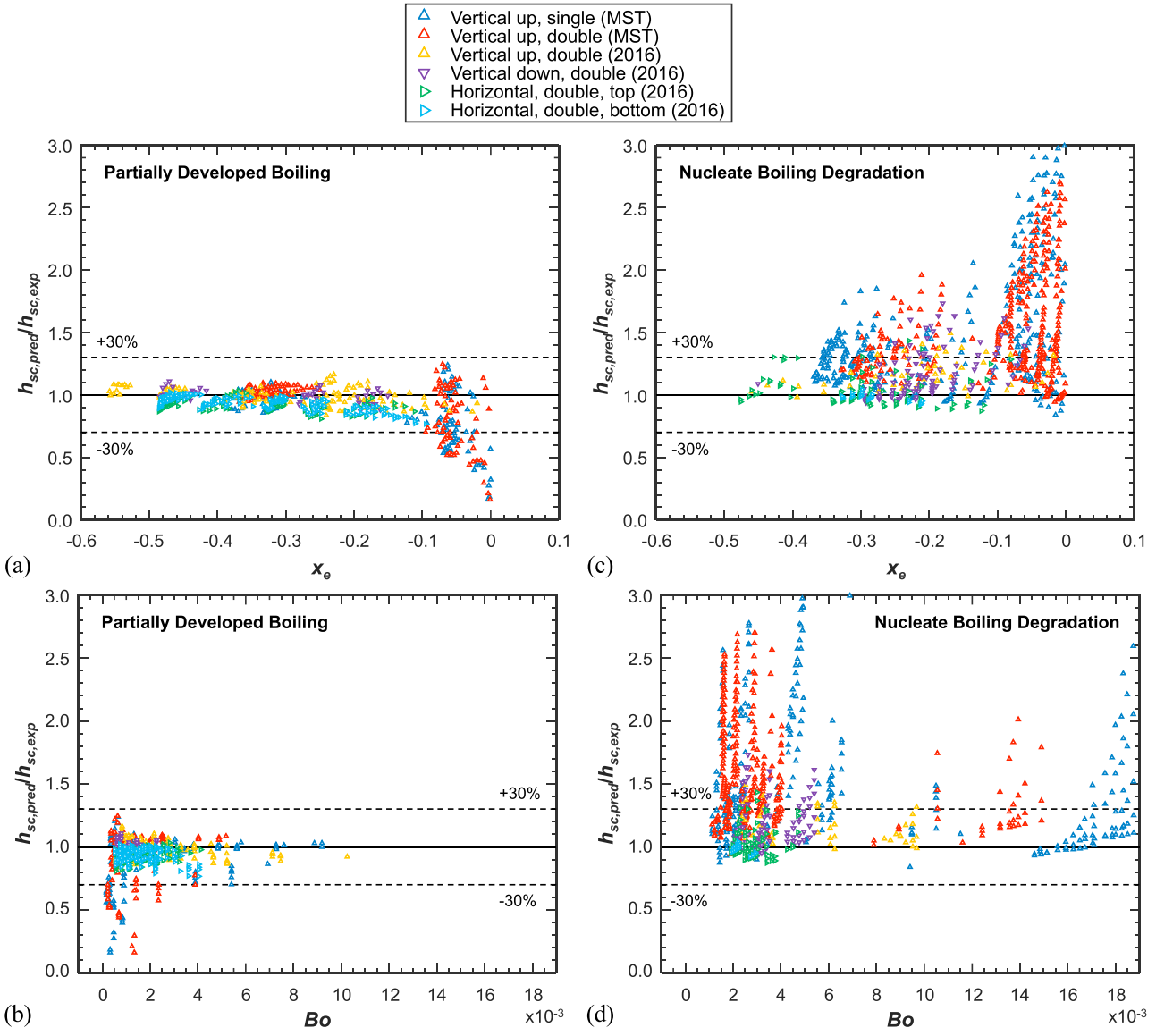

Fig. 13. Prediction trends of new correlation in partially developed boiling regime: (a) $h_{sc,pred}/h_{sc,exp}$ versus x_e and (b) $h_{sc,pred}/h_{sc,exp}$ versus *Bo*, and nucleate boiling degradation regime: (c) $h_{sc,pred}/h_{sc,exp}$ versus x_e and (d) $h_{sc,pred}/h_{sc,exp}$ versus *Bo*. Data markers are segregated for different subsets of the consolidated database.

form predictive capability over the entire subcooling range, and (ii) the most erroneous predictions are in roughly -0.05 < x_e < 0. $h_{sc,pred}/h_{sc,exp}$ versus *Bo* in Fig. 12(c) shows the cluster of datapoints is horizontal meaning the correlation properly incorporates the effects of *Bo*. Fig. 12(c) also confirms the correlation predicts the entire *Bo* range with uniform error.

It is noted that even though Re_{fo} = 966.7 – 26043.83 (Table 4) and the Dittus-Boelter equation in Eq. (11) is recommended for Re_{fo} > 2100 [65], use of the new correlation in Eq. (13) along with Dittus-Boelter equation does not produce any different prediction errors/trends at low Re_{fo} values (past researchers have done this as well for flow boiling, *e.g.*, [64] uses Dittus-Boelter for 57 < Re_{fo} < 49820). This could be due to any possible errors at low Re_{fo} being (i) inconsequential to flow boiling predictions due to the domination of latent heat transfer or (ii) automatically made up for during regression of the developed flow boiling correlation.

Finally, since the new correlation is shown to be independent of both flow orientation and heating configuration, the authors expect the same to be valid for all orientations in Earth gravity and wherever the channel is heated. However, its validity for microgravity conditions will be assessed in the near future using data from FBCE's ISS experiments.

4.5. Extension of new correlation to entire subcooled boiling database

An assessment is made on the predictive capability of the new correlation for the entire subcooled boiling database in Table 2. This means an extension of the new correlation to the PDB and NBD regimes, and the respective prediction statistics are shown in Table 6(a) and 6(b).

The correlation predicts the PDB regime with almost the same accuracy as FDB as evident from an overall MAE of 9.59%. This is consistent with seminal dimensionless group correlations [28,29,31,32], which are applicable to the entire subcooled boiling regime without the need for demarcation. The present errors are higher for the MST data than the 2016 data. Upon assessing the plot of $h_{sc,pred}/h_{sc,exp}$ versus x_e in Fig. 13(a), only the MST datapoints lie outside the ±30%-error band and these highly erroneous datapoints all belong to -0.09 < x_e < 0, where experimental uncertainties are large as already discussed in Section 4.4. Fig. 13(b) shows

predictions with respect to *Bo* are similar to FDB in Fig. 12(c), but the *Bo* range is narrower due to PDB occurring at relatively low *Bo*. Once again, neither flow orientation nor heating configuration has any significant impact on heat transfer in this regime.

On the other hand, the correlation yields very poor predictions for the NBD regime as evident from an overall MAE of 41.71%. Once again, the errors are large for the MST data because of (i) several near-saturated datapoints (see Fig. 13(c)) and (ii) the MST experiments were conducted with comparatively finer heat flux increments near q''_{CHF} to accurately capture CHF, resulting in more NBD datapoints and a bias in count. The correlation overpredicts all datapoints because its present formulation does not account for the physics of degradation. Each streak of datapoints in Fig. 13(d) corresponds to similar operating conditions, where the predictions at the 0%-error line correspond to ONBD and the furthest predictions correspond to heat fluxes near CHF.

The overall prediction results of the new correlation for each regime are shown in Fig. 14, with data markers segregated based on experimental inlet conditions and associated statistics. This enables comparison of trends and numbers with the prior correlations shown in Fig. 5. Overall, the new correlation clearly outperforms all prior seminal correlations for all three regimes, evident by an overall MAE of 20.06% for the entire consolidated database, of which highly subcooled inlet has a MAE of 10.95% and near-saturated inlet 42.07%. 80.86% of the entire database is predicted within ±30%. Excellent predictions can be expected for both partially and fully developed boiling regimes, *i.e.*, the regimes between ONB and ONBD. On the other hand, in practice, one should expect worse overpredictions for the NBD regime, so one should be more careful; first q''_{CHF} should be calculated using a predictive model [47,50] or correlation [51] and heat transfer predictions using the present correlation in the range between ~70-80% and 100% q''_{CHF} should be treated as an upper limit rather than the actual value.

5. Conclusions

This study explored subcooled flow boiling of nPFH in a rectangular channel of 5.0-mm × 2.5-mm cross section at different orientations in Earth gravity (vertical upflow, vertical downflow, and horizontal flow) and partially heated (single-sided and double-sided). Locally subcooled flow boiling datapoints from prior FBCE experiments were consolidated into a single large database spanning broad ranges of operating conditions, flow orientations, and heating configurations. Key conclusions are:

(1) Assessment of prior seminal correlations for this consolidated database revealed the large errors in predictions by all. Amongst all, Moles and Shaw's correlation performed the best with an overall MAE of 37.20%.
(2) Each local flow boiling curve in the database was analyzed, physics discussed, and manually demarcated into partially developed boiling (FDB), fully developed boiling (FDB), and nucleate boiling degradation (NBD) regimes.
(3) A simple to use, yet highly effective correlation of the dimensionless group type is developed for fully developed subcooled flow boiling. The correlation predicts the heat transfer enhancement by subcooled boiling over pure single-phase liquid convection, Eq. (13). Along with the Dittus-Boelter correlation for turbulent single-phase Nusselt number, Eq. (11), the heat transfer coefficient for subcooled flow boiling can be predicted. Both equations are fully explicit functions without artificial singularities. The overall MAE is 6.91% and RMSE is 8.95%, and 91.29% and 99.37% of all FDB datapoints are respectively predicted within errors of ±15% and ±30%.

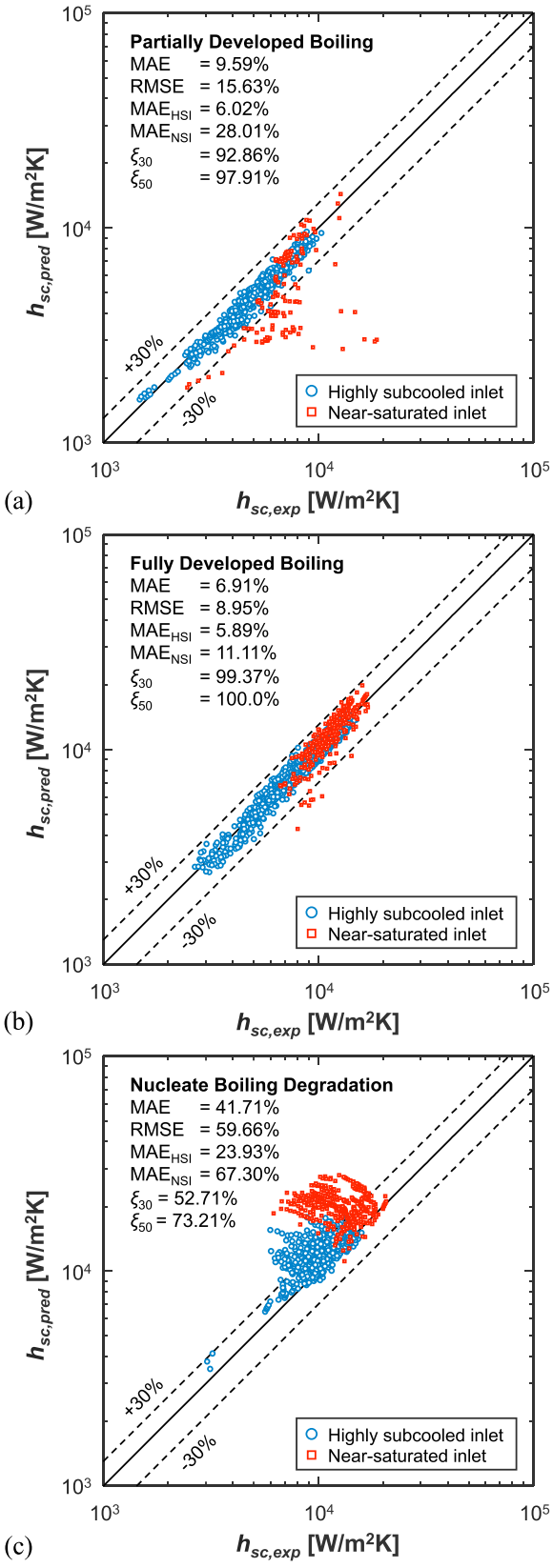

Fig. 14. Parity plots assessing the predictive performance of new correlation for different regimes of subcooled flow boiling: (a) partially developed boiling, (b) fully developed boiling, and (c) nucleate boiling degradation.

Table 6(a)
Prediction statistics for the new correlation in partially developed subcooled flow boiling regime.

Flow orientation	Heating configuration (dataset)	*N*	*MAE*	*RMSE*	ξ_{15}	ξ_{30}
Vertical upflow	Single-sided (MST)	167	14.78%	23.71%	67.66%	80.84%
	Double-sided (MST)	149	13.75%	21.99%	73.83%	82.55%
	Double-sided (2016)	127	5.55%	6.88%	98.43%	100.0%
Vertical downflow	Double-sided (2016)	47	3.84%	5.06%	100.0%	100.0%
Horizontal flow	Double-sided: Top wall (2016)	146	7.96%	9.06%	92.47%	100.0%
	Double-sided: Bottom wall (2016)	176	6.96%	8.69%	90.91%	100.0%
Overall		**812**	**9.59%**	**15.63%**	**84.98%**	**92.86%**

Table 6(b)
Prediction statistics for the new correlation in subcooled flow nucleate boiling degradation regime.

Flow orientation	Heating configuration (dataset)	*N*	*MAE*	*RMSE*	ξ_{15}	ξ_{30}
Vertical upflow	Single-sided (MST)	323	51.52%	71.35%	25.08%	43.96%
	Double-sided (MST)	352	52.03%	66.02%	13.64%	38.92%
	Double-sided (2016)	53	16.77%	20.75%	50.94%	79.25%
Vertical downflow	Double-sided (2016)	94	19.14%	26.55%	56.38%	74.47%
Horizontal flow	Double-sided: Top wall (2016)	80	9.41%	13.07%	85.00%	93.75%
	Double-sided: Bottom wall (2016)	20	2.96%	3.68%	100.0%	100.0%
Overall		**922**	**41.71%**	**59.66%**	**32.21%**	**52.71%**

(4) Upon assessing the correlation's predictions for the other two regimes, the new correlation is equally applicable for PDB and, to a much lesser extent, for NBD. PDB was well predicted with an overall MAE of 9.59% and 92.86% of datapoints within ±30%-error, with the large predictive error mainly due to large experimental uncertainties in the near-saturated regime. This shows the correlation is excellent for both PDB and FDB regimes, meaning its directly applicable for heat fluxes between ONB and ONBD. The predictions are poor for the NBD regime with an overall MAE of 41.71% and only 52.71% of datapoints predicted within ±30%-error. However, the predictions provided by the new correlation can be treated as an upper limit to heat transfer coefficient for heat fluxes between ONBD and CHF, with the actual heat transfer coefficient being increasingly smaller as heat flux is increased from ONBD to CHF.

(5) Comparatively, the new correlation clearly outperforms all prior seminal correlations for the entire consolidated database with an overall MAE of 20.06%, with excellent predictions for both partially and fully developed subcooled flow boiling, Table 4. Moreover, it can be used irrespective of both flow orientation in Earth gravity and heating configuration.

Declaration of Competing Interest

None. The authors declare that they have no known competing financial interests or personal relationships that could have appeared to influence the work reported in this paper.

Data Availability

The data that has been used is confidential.

Acknowledgement

The authors are appreciative of the support of the National Aeronautics and Space Administration (NASA) under grant no. 80NSSC22K0328. The authors sincerely thank their collaborators at the NASA Glenn Research Center, especially Henry K. Nahra, R. Balasubramaniam, Mohammad M. Hasan, and Jeffrey R. Mackey, for their continued efforts in this project. This work was also supported by Purdue University's Bilsland Dissertation Fellowship.

References

[1] I. Mudawar, R.A. Houpt, Mass and momentum transport in smooth falling liquid films laminarized at relatively high Reynolds numbers, Int. J. Heat Mass Transfer 36 (14) (1993) 3437–3448, doi:10.1016/0017-9310(93)90162-Y.

[2] I. Mudawar, T.M. Anderson, Parametric investigation into the effects of pressure, subcooling, surface augmentation and choice of coolant on pool boiling in the design of cooling systems for high-power-density electronic chips, J. Electron. Packag. 112 (4) (1990) 375–382, doi:10.1115/1.2904392.

[3] V.S. Devahdhanush, Y. Lei, Z. Chen, I. Mudawar, Assessing advantages and disadvantages of macro- and micro-channel flow boiling for high-heat-flux thermal management using computational and theoretical/empirical methods, Int. J. Heat Mass Transfer 169 (2021) 120787, doi:10.1016/j.ijheatmasstransfer.2020.120787.

[4] L.E. O'Neill, I. Mudawar, M.M. Hasan, H.K. Nahra, R. Balasubramaniam, N.R. Hall, A. Lokey, J.R. Mackey, Experimental investigation into the impact of density wave oscillations on flow boiling system dynamic behavior and stability, Int. J. Heat Mass Transfer 120 (2018) 144–166, doi:10.1016/j.ijheatmasstransfer.2017.12.011.

[5] S. Lee, V.S. Devahdhanush, I. Mudawar, Pressure drop characteristics of large length-to-diameter two-phase micro-channel heat sinks, Int. J. Heat Mass Transfer 115 (2017) 1258–1275, doi:10.1016/j.ijheatmasstransfer.2017.08.104.

[6] S. Mukherjee, I. Mudawar, Pumpless loop for narrow channel and micro-channel boiling, J. Electron. Packag. 125 (3) (2003) 431–441, doi:10.1115/1.1602708.

[7] V.S. Devahdhanush, S. Lee, I. Mudawar, Experimental investigation of subcooled flow boiling in annuli with reference to thermal management of ultra-fast electric vehicle charging cables, Int. J. Heat Mass Transfer 172 (2021) 121176, doi:10.1016/j.ijheatmasstransfer.2021.121176.

[8] W.P. Klinzing, J.C. Rozzi, I. Mudawar, Film and transition boiling correlations for quenching of hot surfaces with water sprays, J. Heat Treat. 9 (2) (1992) 91–103, doi:10.1007/BF02833145.

[9] M.E. Johns, I. Mudawar, An ultra-high power two-phase jet-impingement avionic clamshell module, J. Electron. Packag. 118 (4) (1996) 264–270, doi:10.1115/1.2792162.

[10] V.S. Devahdhanush, I. Mudawar, Critical heat flux of confined round single jet and jet array impingement boiling, Int. J. Heat Mass Transfer 169 (2021) 120857, doi:10.1016/j.ijheatmasstransfer.2020.120857.

[11] M.K. Sung, I. Mudawar, CHF determination for high-heat flux phase change cooling system incorporating both micro-channel flow and jet impingement, Int. J. Heat Mass Transfer 52 (3–4) (2009) 610–619, doi:10.1016/j.ijheatmasstransfer.2008.07.035.

[12] F.P. Chiaramonte, J.A. Joshi, Workshop on critical issues in microgravity fluids, transport, and reaction processes in advanced human support technology - Final report, TM-2004-212940, NASA, Washington, DC, USA, 2004.

[13] National Research CouncilRecapturing a Future for Space Exploration, The National Academies Press, Washington, DC, USA, 2011, doi:10.17226/13048.

[14] Y.F. Xue, J.F. Zhao, J.J. Wei, J. Li, D. Guo, S.X. Wan, Experimental study of nucleate pool boiling of FC-72 on smooth surface under microgravity, Microgravity Sci. Technol. 23 (2011) 75–85, doi:10.1007/s12217-011-9274-5.

[15] C. Konishi, H. Lee, I. Mudawar, M.M. Hasan, H.K. Nahra, N.R. Hall, J.D. Wagner, R.L. May, J.R. Mackey, Flow boiling in microgravity: Part 1 – Interfacial behavior and experimental heat transfer results, Int. J. Heat Mass Transfer 81 (2015) 705–720, doi:10.1016/j.ijheatmasstransfer.2014.10.049.

[16] A. Weinzierl, J. Straub, Nucleate pool boiling in microgravity environment, in: Proc. Int. Heat Transfer Conf, 7, Begell House Inc., Munich, Germany, 1982, pp. 21–27, doi:10.1615/IHTC7.3730.

[17] V.K. Dhir, G.R. Warrier, E. Aktinol, D. Chao, J. Eggers, W. Sheredy, W. Booth, Nucleate pool boiling experiments (NPBX) on the International Space Station, Microgravity Sci. Technol. 24 (5) (2012) 307–325, doi:10.1007/s12217-012-9315-8.

[18] H. Zhang, I. Mudawar, M.M. Hasan, Experimental and theoretical study of orientation effects on flow boiling CHF, Int. J. Heat Mass Transfer 45 (22) (2002) 4463–4477, doi:10.1016/S0017-9310(02)00152-7.
[19] H. Zhang, I. Mudawar, M.M. Hasan, A method for assessing the importance of body force on flow boiling CHF, J. Heat Transfer 126 (2) (2004) 161–168, doi:10.1115/1.1651532.
[20] L.E. O'Neill, I. Park, C.R. Kharangate, V.S. Devahdhanush, V. Ganesan, I. Mudawar, Assessment of body force effects in flow condensation, part II: Criteria for negating influence of gravity, Int. J. Heat Mass Transfer 106 (2017) 313–328, doi:10.1016/j.ijheatmasstransfer.2016.07.019.
[21] V.S. Devahdhanush, S. Lee, I. Mudawar, Consolidated theoretical/empirical predictive method for subcooled flow boiling in annuli with reference to thermal management of ultra-fast electric vehicle charging cables, Int. J. Heat Mass Transfer 175 (2021) 121224, doi:10.1016/j.ijheatmasstransfer.2021.121224.
[22] V.S. Devahdhanush, I. Mudawar, H.K. Nahra, R. Balasubramaniam, M.M. Hasan, J.R. Mackey, Experimental heat transfer results and flow visualization of vertical upflow boiling in Earth gravity with subcooled inlet conditions – In preparation for experiments onboard the International Space Station, Int. J. Heat Mass Transfer 188 (2022) 122603, doi:10.1016/j.ijheatmasstransfer.2022.122603.
[23] W.H. McAdams, W.E. Kennel, C.S. Minden, R. Carl, P.M. Picornell, J.E. Dew, Heat transfer at high rates to water with surface boiling, Ind. Eng. Chem. 41 (9) (1949) 1945–1953, doi:10.1021/ie50477a027.
[24] W.H. Jens, P.A. Lottes, Analysis of heat transfer, burnout, pressure drop and density data for high-pressure water, Report No. ANL-4627, Argonne National Lab, Lemont, IL, USA, 1951.
[25] J.R.S. Thom, W.M. Walker, T.A. Fallon, G.F.S. Reising, Boiling in sub-cooled water during flow up heated tubes or annuli, Proc. Inst. Mech. Eng. 180 (3C) (1965) 226–246, doi:10.1243/PIME_CONF_1965_180_117_02.
[26] M. Araki, M. Ogawa, T. Kunugi, K. Satoh, S. Suzuki, Experiments on heat transfer of smooth and swirl tubes under one-sided heating conditions, Int. J. Heat Mass Transfer 39 (14) (1996) 3045–3055, doi:10.1016/0017-9310(95)00344-4.
[27] K. Hata, S. Masuzaki, Subcooled boiling heat transfer for turbulent flow of water in a short vertical tube, J. Heat Transfer 132 (1) (2010) 1–11, doi:10.1115/1.3194768.
[28] S.S. Papell, Subcooled boiling heat transfer under forced convection in a heated tube, NASA Technical Note D-1583, Lewis Research Center, Cleveland, OH, USA, 1963.
[29] M. Badiuzzaman, Correlation of subcooled boiling data, Pak. Eng. 7 (1967) 759–764.
[30] A.S. Hodgson, PhD Thesis, University of London, London, UK, 1966.
[31] F.D. Moles, J.F.G. Shaw, Boiling heat transfer to sub-cooled liquids under conditions of forced convection, Trans. Inst. Chem. Eng. 50 (1) (1972) 76–84.
[32] J. Shaw, PhD Thesis, Chemical Engineering, University of Surrey, Guildford, Surrey, UK, 1972.
[33] J.C. Chen, Correlation for boiling heat transfer to saturated fluids in convective flow, Ind. Eng. Chem. Process Des. Dev. 5 (3) (1966) 322–329, doi:10.1021/i260019a023.
[34] R.W. Bjorg, G.R. Hall, W.M. Rohsenow, Correlation of forced convection boiling heat transfer data, Int. J. Heat Mass Transfer 25 (6) (1982) 753–757, doi:10.1016/0017-9310(82)90087-4.
[35] K.E. Gungor, R.H.S. Winterton, A general correlation for flow boiling in tubes and annuli, Int. J. Heat Mass Transfer 29 (3) (1986) 351–358, doi:10.1016/0017-9310(86)90205-X.
[36] Z. Liu, R.H.S. Winterton, A general correlation for saturated and subcooled flow boiling in tubes and annuli, based on a nucleate pool boiling equation, Int. J. Heat Mass Transfer 34 (11) (1991) 2759–2766, doi:10.1016/0017-9310(91)90234-6.
[37] M.M. Shah, A general correlation for heat transfer during subcooled boiling in pipes and annuli, ASHRAE Trans 83 (1) (1977) 202–217.
[38] M.M. Shah, New correlation for heat transfer during subcooled boiling in plain channels and annuli, Int. J. Therm. Sci. 112 (2017) 358–370, doi:10.1016/j.ijthermalsci.2016.10.016.
[39] V. Prodanovic, D. Fraser, M. Salcudean, On the transition from partial to fully developed subcooled flow boiling, Int. J. Heat Mass Transfer 45 (24) (2002) 4727–4738, doi:10.1016/S0017-9310(02)00197-7.
[40] P.K. Baburajan, G.S. Bisht, S.K. Gupta, S.V. Prabhu, Measurement of subcooled boiling pressure drop and local heat transfer coefficient in horizontal tube under LPLF conditions, Nucl. Eng. Des. 255 (2013) 169–179, doi:10.1016/j.nucengdes.2012.10.012.
[41] S. Hua, R. Huang, Z. Li, P. Zhou, Experimental study on the heat transfer characteristics of subcooled flow boiling with cast iron heating surface, Appl. Therm. Eng. 77 (2015) 180–191, doi:10.1016/j.applthermaleng.2014.11.082.
[42] J. Yan, Q. Bi, Z. Liu, G. Zhu, L. Cai, Subcooled flow boiling heat transfer of water in a circular tube under high heat fluxes and high mass fluxes, Fusion Eng. Des. 100 (2015) 406–418, doi:10.1016/j.fusengdes.2015.07.007.
[43] G. Zhu, Q. Bi, J. Yan, H. Lv, Experimental study of subcooled flow boiling heat transfer of water in a circular channel under one-side heating conditions, Int. J. Heat Mass Transfer 119 (2018) 484–495, doi:10.1016/j.ijheatmasstransfer.2017.11.111.
[44] Z. Chen, W. Li, J. Li, K. Zhou, Z. Feng, A new correlation for subcooled flow boiling heat transfer in a vertical narrow microchannel, J. Electron. Packag. 143 (1) (2021) 014501, doi:10.1115/1.4046755.
[45] B.S. Haynes, D.F. Fletcher, Subcooled flow boiling heat transfer in narrow passages, Int. J. Heat Mass Transfer 46 (19) (2003) 3673–3682, doi:10.1016/S0017-9310(03)00172-8.
[46] J. Lee, I. Mudawar, Fluid flow and heat transfer characteristics of low temperature two-phase micro-channel heat sinks - Part 2. Subcooled boiling pressure drop and heat transfer, Int. J. Heat Mass Transfer 51 (17–18) (2008) 4327–4341, doi:10.1016/j.ijheatmasstransfer.2008.02.013.
[47] V.S. Devahdhanush, S.J. Darges, I. Mudawar, H.K. Nahra, R. Balasubramaniam, M.M. Hasan, J.R. Mackey, Flow visualization, heat transfer, and critical heat flux of flow boiling in Earth gravity with saturated liquid-vapor mixture inlet conditions – In preparation for experiments onboard the International Space Station, Int. J. Heat Mass Transfer 192 (2022) 122890, doi:10.1016/j.ijheatmasstransfer.2022.122890.
[48] C.R. Kharangate, L.E. O'Neill, I. Mudawar, M.M. Hasan, H.K. Nahra, R. Balasubramaniam, N.R. Hall, A.M. Macner, J.R. Mackey, Effects of subcooling and two-phase inlet on flow boiling heat transfer and critical heat flux in a horizontal channel with one-sided and double-sided heating, Int. J. Heat Mass Transfer 91 (2015) 1187–1205, doi:10.1016/j.ijheatmasstransfer.2015.08.059.
[49] C.R. Kharangate, C. Konishi, I. Mudawar, Consolidated methodology to predicting flow boiling critical heat flux for inclined channels in Earth gravity and for microgravity, Int. J. Heat Mass Transfer 92 (2016) 467–482, doi:10.1016/j.ijheatmasstransfer.2015.08.018.
[50] S.J. Darges, V.S. Devahdhanush, I. Mudawar, H.K. Nahra, R. Balasubramaniam, M.M. Hasan, J.R. Mackey, Experimental results and interfacial lift-off model predictions of critical heat flux for flow boiling with subcooled inlet conditions – In preparation for experiments onboard the International Space Station, Int. J. Heat Mass Transfer 183 (2022) 122241, doi:10.1016/j.ijheatmasstransfer.2021.122241.
[51] S.J. Darges, V.S. Devahdhanush, I. Mudawar, Assessment and development of flow boiling critical heat flux correlations for partially heated rectangular channels in different gravitational environments, Int. J. Heat Mass Transfer (2022) under review.
[52] L.E. O'Neill, I. Mudawar, M.M. Hasan, H.K. Nahra, R. Balasubramaniam, J.R. Mackey, Experimental investigation of frequency and amplitude of density wave oscillations in vertical upflow boiling, Int. J. Heat Mass Transfer 125 (2018) 1240–1263, doi:10.1016/j.ijheatmasstransfer.2018.04.138.
[53] W.A. Arnold, T.G. Hartman, J. McQuillen, Chemical characterization and thermal stressing studies of perfluorohexane fluids for space-based applications, J. Spacecr. Rockets 44 (1) (2007) 94–102, doi:10.2514/1.22537.
[54] S. Lee, V.S. Devahdhanush, I. Mudawar, Experimental and analytical investigation of flow loop induced instabilities in micro-channel heat sinks, Int. J. Heat Mass Transfer 140 (2019) 303–330, doi:10.1016/j.ijheatmasstransfer.2019.05.077.
[55] E.W. Lemmon, I.H. Bell, M.L. Huber, M.O. McLinden, NIST Standard Reference Database 23: Reference Fluid Thermodynamic and Transport Properties-REFPROP, Version 10, NIST, Gaithersburg, MD, USA, 2018.
[56] F.W. Dittus, L.M.K. Boelter, Heat transfer in automobile radiators of the tubular type, Int. Commun. Heat Mass Transfer 12 (1) (1985) 3–22, doi:10.1016/0735-1933(85)90003-X.
[57] R.H.S. Winterton, Where did the Dittus and Boelter equation come from? Int. J. Heat Mass Transfer 41 (4–5) (1998) 809–810, doi:10.1016/S0017-9310(97)00177-4.
[58] E.N. Sieder, G.E. Tate, Heat transfer and pressure drop of liquids in tubes, Ind. Eng. Chem. 28 (12) (1936) 1429–1435, doi:10.1021/ie50324a027.
[59] V.S. Devahdhanush, I. Mudawar, Review of critical heat flux (CHF) in jet impingement boiling, Int. J. Heat Mass Transfer 169 (2021) 120893, doi:10.1016/j.ijheatmasstransfer.2020.120893.
[60] M.G. Cooper, Saturation nucleate pool boiling - A simple correlation, in: First UK Natl. Conf. Heat Transfer, IChemE Symp. Ser., 2.86, IChemE, Woodhouse, Leeds, UK, 1984, pp. 785–793, doi:10.1016/b978-0-85295-175-0.50013-8.
[61] S. Lee, V.S. Devahdhanush, I. Mudawar, Investigation of subcooled and saturated boiling heat transfer mechanisms, instabilities, and transient flow regime maps for large length-to-diameter ratio micro-channel heat sinks, Int. J. Heat Mass Transfer 123 (2018) 172–191, doi:10.1016/j.ijheatmasstransfer.2018.02.020.
[62] P.W. Holland, R.E. Welsch, Robust regression using iteratively reweighted least-squares, Commun. Stat.- Theory Methods 6 (9) (1977) 813–827, doi:10.1080/03610927708827533.
[63] H.J. Seltman, Experimental Design and Analysis, Department of Statistics, Carnegie Mellon University, 2018 Book only available online at http://www.stat.cmu.edu/~hseltman/309/Book/Book.pdf.
[64] S.M. Kim, I. Mudawar, Universal approach to predicting saturated flow boiling heat transfer in mini/micro-channels – Part II. Two-phase heat transfer coefficient, Int. J. Heat Mass Transfer 64 (2013) 1239–1256, doi:10.1016/j.ijheatmasstransfer.2013.04.014.
[65] W.H. McAdams, Heating and cooling inside tubes, in: Heat Transmission, 2nd ed., McGraw-Hill Book Company Inc., New York, NY, USA, 1942, pp. 154–209.
[66] A.P. Colburn, A method of correlating forced convection heat-transfer data and a comparison with fluid friction, Int. J. Heat Mass Transfer 7 (12) (1964) 1359–1384, doi:10.1016/0017-9310(64)90125-5.